



CERN-PH-EP-2014-019

Submitted to: JHEP

Search for direct production of charginos and neutralinos in events with three leptons and missing transverse momentum in $\sqrt{s} = 8$ TeV pp collisions with the ATLAS detector

The ATLAS Collaboration

Abstract

A search for the direct production of charginos and neutralinos in final states with three leptons and missing transverse momentum is presented. The analysis is based on 20.3 fb^{-1} of $\sqrt{s} = 8$ TeV proton–proton collision data delivered by the Large Hadron Collider and recorded with the ATLAS detector. Observations are consistent with the Standard Model expectations and limits are set in R -parity-conserving phenomenological Minimal Supersymmetric Standard Models and in simplified supersymmetric models, significantly extending previous results. For simplified supersymmetric models of direct chargino ($\tilde{\chi}_1^\pm$) and next-to-lightest neutralino ($\tilde{\chi}_2^0$) production with decays to lightest neutralino ($\tilde{\chi}_1^0$) via either all three generations of sleptons, staus only, gauge bosons, or Higgs bosons, $\tilde{\chi}_1^\pm$ and $\tilde{\chi}_2^0$ masses are excluded up to 700 GeV, 380 GeV, 345 GeV, or 148 GeV respectively, for a massless $\tilde{\chi}_1^0$.

Search for direct production of charginos and neutralinos in events with three leptons and missing transverse momentum in $\sqrt{s} = 8$ TeV pp collisions with the ATLAS detector

The ATLAS Collaboration

ABSTRACT: A search for the direct production of charginos and neutralinos in final states with three leptons and missing transverse momentum is presented. The analysis is based on 20.3 fb^{-1} of $\sqrt{s} = 8$ TeV proton–proton collision data delivered by the Large Hadron Collider and recorded with the ATLAS detector. Observations are consistent with the Standard Model expectations and limits are set in R -parity-conserving phenomenological Minimal Supersymmetric Standard Models and in simplified supersymmetric models, significantly extending previous results. For simplified supersymmetric models of direct chargino ($\tilde{\chi}_1^\pm$) and next-to-lightest neutralino ($\tilde{\chi}_2^0$) production with decays to lightest neutralino ($\tilde{\chi}_1^0$) via either all three generations of sleptons, staus only, gauge bosons, or Higgs bosons, $\tilde{\chi}_1^\pm$ and $\tilde{\chi}_2^0$ masses are excluded up to 700 GeV, 380 GeV, 345 GeV, or 148 GeV respectively, for a massless $\tilde{\chi}_1^0$.

Contents

1	Introduction	1
2	SUSY scenarios	2
3	The ATLAS detector	4
4	Monte Carlo simulation	4
5	Event reconstruction	5
6	Event selection	7
7	Standard Model background estimation	10
7.1	Irreducible background processes	10
7.2	Reducible background processes	10
7.3	Systematic uncertainties	12
7.4	Background modelling validation	13
8	Results and interpretations	14
9	Conclusions	21
10	Acknowledgements	24

1 Introduction

Supersymmetry (SUSY) [1–9] proposes the existence of supersymmetric particles, with spin differing by one-half unit with respect to that of their Standard Model (SM) partners. Charginos, $\tilde{\chi}_{1,2}^{\pm}$, and neutralinos, $\tilde{\chi}_{1,2,3,4}^0$, collectively referred to as electroweakinos, are the ordered mass eigenstates formed from the linear superposition of the SUSY partners of the Higgs and electroweak gauge bosons (higgsinos, winos and binos). Based on naturalness arguments [10, 11], the lightest electroweakinos are expected to have mass of order 100 GeV and be accessible at the Large Hadron Collider (LHC). In the R -parity-conserving minimal supersymmetric extension of the SM (MSSM) [12–16], SUSY particles are pair-produced and the lightest SUSY particle (LSP), assumed in many models to be the $\tilde{\chi}_1^0$, is stable. Charginos and neutralinos can decay into leptonic final states via superpartners of neutrinos ($\tilde{\nu}$, sneutrinos) or charged leptons ($\tilde{\ell}$, sleptons), or via W , Z or Higgs (h) bosons ($\tilde{\chi}_i^{\pm} \rightarrow \ell^{\pm}\tilde{\nu}, \nu\tilde{\ell}^{\pm}, W^{\pm}\tilde{\chi}_j^0, Z\tilde{\chi}_j^{\pm}, h\tilde{\chi}_j^{\pm}$ and $\tilde{\chi}_i^0 \rightarrow \nu\tilde{\nu}, \ell^{\pm}\tilde{\ell}^{\mp}, W^{\pm}\tilde{\chi}_j^{\mp}, Z\tilde{\chi}_j^0, h\tilde{\chi}_j^0$ respectively).

This paper presents a search performed with the ATLAS detector for the direct production of charginos and neutralinos decaying to a final state with three charged leptons (e ,

μ or τ , referred to as leptons in the following) and missing transverse momentum originating from the two undetected LSPs and the neutrinos. The analysis is based on 20.3 fb^{-1} of proton-proton collision data recorded by ATLAS at a centre-of-mass energy of $\sqrt{s} = 8 \text{ TeV}$. Previous searches for charginos and neutralinos are documented in refs [17–19] by ATLAS, and in ref. [20] by CMS. Similar searches were conducted at the Tevatron [21, 22]. At LEP [23–27], searches for direct chargino production set a model-independent lower limit of 103.5 GeV at 95% confidence level (CL) on the mass of promptly decaying charginos.

2 SUSY scenarios

Among the electroweakino pair-production processes leading to three leptons in the final state, $\tilde{\chi}_1^\pm \tilde{\chi}_2^0$ production has the largest cross-section in most of the MSSM parameter space. Several simplified supersymmetric models (“simplified models” [28]) are considered for the optimisation of the search and interpretation of results. The simplified models target the direct production of $\tilde{\chi}_1^\pm$ and $\tilde{\chi}_2^0$, where the masses and the decay modes of the relevant particles ($\tilde{\chi}_1^\pm$, $\tilde{\chi}_1^0$, $\tilde{\chi}_2^0$, $\tilde{\nu}$, $\tilde{\ell}_L$ ¹) are the only free parameters. It is assumed that the $\tilde{\chi}_1^\pm$ and $\tilde{\chi}_2^0$ consist purely of the wino component and are degenerate in mass, while the $\tilde{\chi}_1^0$ consists purely of the bino component. Four different scenarios for the decay of the $\tilde{\chi}_1^\pm$ and $\tilde{\chi}_2^0$ are considered, where in all cases the decays are prompt,

$\tilde{\ell}_L$ -mediated: the $\tilde{\chi}_1^\pm$ and $\tilde{\chi}_2^0$ decay with a branching fraction of 1/6 via \tilde{e}_L , $\tilde{\mu}_L$, $\tilde{\tau}_L$, $\tilde{\nu}_e$, $\tilde{\nu}_\mu$, or $\tilde{\nu}_\tau$ with masses $m_{\tilde{\nu}} = m_{\tilde{\ell}_L} = (m_{\tilde{\chi}_1^0} + m_{\tilde{\chi}_1^\pm})/2$,

$\tilde{\tau}_L$ -mediated: the first- and second-generation sleptons and sneutrinos are assumed to be heavy, so that the $\tilde{\chi}_1^\pm$ and $\tilde{\chi}_2^0$ decay with a branching fraction of 1/2 via $\tilde{\tau}$ or $\tilde{\nu}_\tau$ with masses $m_{\tilde{\nu}_\tau} = m_{\tilde{\tau}} = (m_{\tilde{\chi}_1^0} + m_{\tilde{\chi}_2^0})/2$,

WZ -mediated: all sleptons and sneutrinos are assumed to be heavy, and the $\tilde{\chi}_1^\pm$ and $\tilde{\chi}_2^0$ decay via $W^{(*)}$ and $Z^{(*)}$ bosons, respectively, with a branching fraction of 100%,

Wh -mediated: all sleptons and sneutrinos are assumed to be heavy, and the $\tilde{\chi}_1^\pm$ and $\tilde{\chi}_2^0$ decay via W and lightest Higgs bosons, respectively, with a branching fraction of 100%. The Higgs boson considered is SM-like, with a mass of 125 GeV and is assumed to decay with SM branching ratios.

Diagrams for the considered $\tilde{\chi}_1^\pm \tilde{\chi}_2^0$ production and decay modes are shown in figure 1.

Results are also interpreted in dedicated phenomenological MSSM (pMSSM) [29] scenarios, which consider all relevant SUSY production processes. In the models considered in this paper, the masses of the coloured sparticles, of the CP-odd Higgs boson, and of the left-handed sleptons are set to high values to allow only the direct production of charginos and neutralinos via W/Z bosons and their decay via right-handed sleptons, gauge bosons and Higgs bosons. By tuning the mixing in the top-squark sector, the value of the lightest Higgs boson mass is set close to 125 GeV, which is consistent with the mass of the observed Higgs boson [30, 31]. The mass hierarchy, composition and production cross-sections of

¹The sleptons are referred to as left- or right-handed (e.g. $\tilde{\ell}_L$ or $\tilde{\ell}_R$), depending on the helicity of the fermionic superpartners.

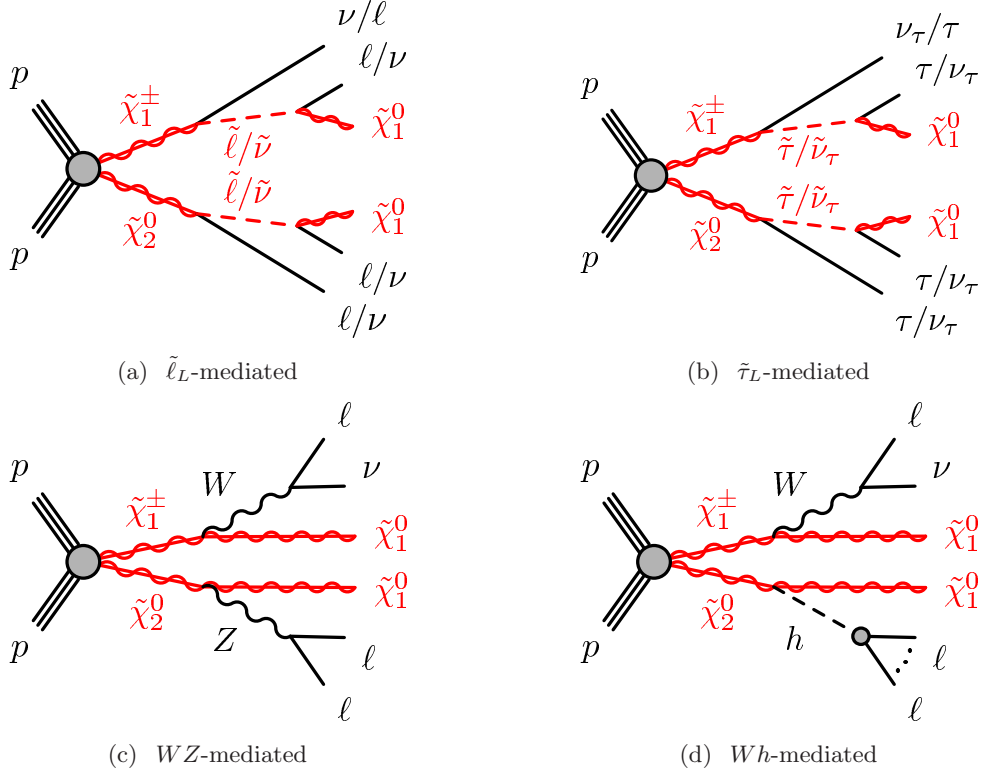


Figure 1. The Feynman diagrams for the four simplified models of the direct production of $\tilde{\chi}_1^\pm \tilde{\chi}_2^0$ studied in this paper. The different decay modes are discussed in the text. The dots in (d) depict possible additional decay products of the lightest Higgs boson decaying via intermediate $\tau\tau$, WW or ZZ states.

the electroweakinos are governed by the ratio of the expectation values of the two Higgs doublets $\tan\beta$, the gaugino mass parameters M_1 and M_2 , and the higgsino mass parameter μ . For the hierarchy $M_1 < M_2 < \mu$ ($M_1 < \mu < M_2$), the $\tilde{\chi}_1^0$ is bino-like, the $\tilde{\chi}_1^\pm$ and $\tilde{\chi}_2^0$ are wino-like (higgsino-like) and the dominant electroweakino production process leading to a final state with three leptons is $pp \rightarrow \tilde{\chi}_1^\pm \tilde{\chi}_2^0$ ($pp \rightarrow \tilde{\chi}_1^\pm \tilde{\chi}_2^0$, $pp \rightarrow \tilde{\chi}_1^\pm \tilde{\chi}_3^0$). If $M_2 < M_1 < \mu$ ($\mu < M_1 < M_2$), the $\tilde{\chi}_1^0$ ($\tilde{\chi}_1^0$, $\tilde{\chi}_2^0$) and the $\tilde{\chi}_1^\pm$ are wino-like (higgsino-like) with similar masses and the dominant process leading to a final state with three high transverse momentum leptons is the pair-production of the higgsino-like (wino-like) $\tilde{\chi}_2^\pm$ and the bino-like $\tilde{\chi}_2^0$ ($\tilde{\chi}_3^0$).

Finally, the pMSSM scenarios under study are parametrised in the μ - M_2 plane and are classified based on the masses of the right-handed sleptons into three groups,

pMSSM $\tilde{\ell}_R$: the right-handed sleptons are degenerate in mass, with mass $m_{\tilde{\ell}_R} = (m_{\tilde{\chi}_1^0} + m_{\tilde{\chi}_2^0})/2$. Setting the parameter $\tan\beta = 6$ yields comparable $\tilde{\chi}_2^0$ branching ratios into each slepton generation. The $\tilde{\chi}_1^\pm$ decays predominantly via a W boson when kinematically allowed and to $\tilde{\tau}$ otherwise because the sleptons are right-handed. To probe the sensitivity for different $\tilde{\chi}_1^0$ compositions, three values of M_1 are considered: 100 GeV, 140 GeV and 250 GeV,

pMSSM $\tilde{\tau}_R$: the selectrons and smuons are heavy and the $\tilde{\tau}_R$ mass is set to $m_{\tilde{\tau}_R} = (m_{\tilde{\chi}_1^0} + m_{\tilde{\chi}_2^0})/2$ and $\tan\beta$ to 50, hence decays via right-handed staus dominate. The parameter M_1 is set to 75 GeV resulting in a bino-like $\tilde{\chi}_1^0$,

pMSSM no $\tilde{\ell}$: all sleptons are heavy so that decays via W , Z or Higgs bosons dominate. The remaining parameters are $M_1 = 50$ GeV and $\tan\beta = 10$. The Higgs branching fractions are SM-like across much of the parameter space considered. However, the $h \rightarrow \tilde{\chi}_1^0 \tilde{\chi}_1^0$ branching fraction rises to $\sim 20\%$ ($\sim 70\%$) when μ decreases to 200 (100) GeV, suppressing other decay modes, but this does not affect the mass limits significantly.

3 The ATLAS detector

The ATLAS detector [32] is a multi-purpose particle physics detector with forward-backward symmetric cylindrical geometry.² The inner tracking detector (ID) covers $|\eta| < 2.5$ and consists of a silicon pixel detector, a semiconductor microstrip detector, and a transition radiation tracker. The ID is surrounded by a thin superconducting solenoid providing a 2 T axial magnetic field. A high-granularity lead/liquid-argon (LAr) sampling calorimeter measures the energy and the position of electromagnetic showers within $|\eta| < 3.2$. Sampling calorimeters with LAr are also used to measure hadronic showers in the end-cap ($1.5 < |\eta| < 3.2$) and forward ($3.1 < |\eta| < 4.9$) regions, while an iron/scintillator tile calorimeter measures hadronic showers in the central region ($|\eta| < 1.7$). The muon spectrometer (MS) surrounds the calorimeters and consists of three large superconducting air-core toroid magnets, each with eight coils, a system of precision tracking chambers ($|\eta| < 2.7$), and fast trigger chambers ($|\eta| < 2.4$). A three-level trigger system [33] selects events to be recorded for offline analysis.

4 Monte Carlo simulation

Monte Carlo (MC) generators are used to simulate SM processes and new physics signals relevant to this analysis. The SM processes considered are those that can lead to leptonic signatures. The diboson production processes considered include WW , WZ and ZZ (where “ Z ” also includes virtual photons), and the $W\gamma$ and $Z\gamma$ processes. The triboson processes considered are WWW and ZWW (collectively referred to as VVV), while samples of SM Higgs boson production via gluon fusion, vector-boson-fusion or in association with W/Z bosons or $t\bar{t}$ are also studied. The $t\bar{t}$, single top-quark, W +jets, Z +jets, $t\bar{t}W$, $t\bar{t}Z$, $t\bar{t}WW$, and tZ processes are also considered, where $t\bar{t}W$, $t\bar{t}Z$ and $t\bar{t}WW$ are collectively referred to as $t\bar{t}V$. Details of the MC simulation samples used in this paper, as well as the order of cross-section calculations in perturbative QCD used for yield normalisation are shown in table 1.

²ATLAS uses a right-handed coordinate system with its origin at the nominal interaction point (IP) in the centre of the detector and the z -axis along the beam pipe. The x -axis points from the IP to the centre of the LHC ring, and the y -axis points upward. Cylindrical coordinates (r, ϕ) are used in the transverse plane, ϕ being the azimuthal angle around the z -axis. The pseudorapidity is defined in terms of the polar angle θ as $\eta = -\ln \tan(\theta/2)$.

Table 1. For the MC samples used in this paper for background estimates, the generator type, the order of cross-section calculations used for yield normalisation, names of parameter tunes used for the underlying event generation and PDF sets.

Process	Generator + fragmentation/hadronisation	Cross-section	Tune	PDF set
Dibosons				
WW, WZ, ZZ	POWHEG-r2129 [34, 35] + PYTHIA-8.165 [38]	NLO QCD with MCFM-6.2 [39, 40]	AU2 [36]	CT10 [37]
* WZ, ZZ	aMC@NLO-2.0.0.beta3 [41] + HERWIG-6.520 [42] (or + PYTHIA-6.426)	NLO QCD with MCFM-6.2	AU2	CT10
ZZ via gluon fusion (not incl. in POWHEG)	gg2VV [43] + HERWIG-6.520	NLO	AUET2B [44]	CT10
$W\gamma, Z\gamma$	SHERPA-1.4.1 [45]	NLO	(internal)	CT10
Tribosons				
WWW, ZWW	MADGRAPH-5.0 [46] + PYTHIA-6.426	NLO [47]	AUET2B	CTEQ6L1 [48]
Higgs				
via gluon fusion	POWHEG-r2092 + PYTHIA-8.165	NNLL QCD, NLO EW [49]	AU2	CT10
via vector-boson-fusion	POWHEG-r2092 + PYTHIA-8.165	NNLO QCD, NLO EW [49]	AU2	CT10
associated W/Z production	PYTHIA-8.165	NNLO QCD, NLO EW [49]	AU2	CTEQ6L1
associated $t\bar{t}$ -production	PYTHIA-8.165	NNLO QCD [49]	AU2	CTEQ6L1
Top+Boson				
$t\bar{t}W, t\bar{t}Z$	ALPGEN-2.14 [50] + HERWIG-6.520	NLO [51, 52]	AUET2B	CTEQ6L1
* $t\bar{t}W, t\bar{t}Z$	MADGRAPH-5.0 + PYTHIA-6.426	NLO	AUET2B	CTEQ6L1
$t\bar{t}WW$	MADGRAPH-5.0 + PYTHIA-6.426	NLO [52]	AUET2B	CTEQ6L1
tZ	MADGRAPH-5.0 + PYTHIA-6.426	NLO [53]	AUET2B	CTEQ6L1
$t\bar{t}$	POWHEG-r2129 + PYTHIA-6.426	NNLO+NNLL [54–59]	PERUGIA2011C	CT10
Single top				
t -channel	ACERMC-38 [60] + PYTHIA-6.426	NNLO+NNLL [61]	AUET2B	CTEQ6L1
s -channel, Wt	MC@NLO-4.06 [62, 63] + HERWIG-6.520	NNLO+NNLL [64, 65]	AUET2B	CT10
W+jets, Z+jets	ALPGEN-2.14 + PYTHIA-6.426 (or + HERWIG-6.520)	DYNNLO-1.1 [66] with MSTW2008 NNLO [67]	PERUGIA2011C	CTEQ6L1

For all MC samples, the propagation of particles through the ATLAS detector is modelled with GEANT4 [68] using the full ATLAS detector simulation [69], except the $t\bar{t}$ POWHEG sample, for which a fast simulation using a parametric response of the electromagnetic and hadronic calorimeters is used [70]. The effect of multiple proton–proton collisions from the same or nearby beam bunch crossings (in-time or out-of-time pile-up) is incorporated into the simulation by overlaying additional minimum-bias events generated with PYTHIA onto hard-scatter events. Simulated events are weighted to match the distribution of the number of interactions per bunch crossing observed in data, but are otherwise reconstructed in the same manner as data.

The SUSY signal samples are produced with HERWIG++-2.5.2 [71] using the CTEQ6L1 PDF set. Signal cross-sections are calculated to NLO in the strong coupling constant using PROSPINO2 [72]. They are in agreement with the NLO calculations matched to resummation at next-to-leading logarithmic accuracy (NLO+NNLL) within $\sim 2\%$ [73–75]. The nominal cross-section and the uncertainty are taken from the center and spread, respectively, of the envelope of cross-section predictions using different PDF sets and factorisation and renormalisation scales, as described in ref. [76].

5 Event reconstruction

Events recorded during stable data-taking conditions are analysed if the primary vertex has five or more tracks with transverse momentum $p_T > 400$ MeV associated with it. The

primary vertex of an event is identified as the vertex with the highest Σp_T^2 of associated tracks. After the application of beam, detector and data-quality requirements, the total luminosity considered in this analysis corresponds to 20.3 fb^{-1} .

Electron candidates must satisfy “medium” identification criteria, following ref. [77] (modified for 2012 data conditions), and are required to have $|\eta| < 2.47$ and $p_T > 10 \text{ GeV}$. Electron p_T and $|\eta|$ are determined from the calibrated clustered energy deposits in the electromagnetic calorimeter and the matched ID track, respectively. Muon candidates are reconstructed by combining tracks in the ID and tracks in the MS [78] and are required to have $|\eta| < 2.5$ and $p_T > 10 \text{ GeV}$. Events containing one or more muons that have transverse impact parameter with respect to the primary vertex $|d_0| > 0.2 \text{ mm}$ or longitudinal impact parameter with respect to the primary vertex $|z_0| > 1 \text{ mm}$ are rejected to suppress cosmic-ray muon background.

Jets are reconstructed with the anti- k_t algorithm [79] with a radius parameter of $\Delta R \equiv \sqrt{(\Delta\phi)^2 + (\Delta\eta)^2} = 0.4$ using three-dimensional calorimeter energy clusters as input. The clusters are calibrated using the so-called local hadronic calibration, which consists of weighting differently the energy deposits arising from the electromagnetic and hadronic components of the showers [33]. The final jet energy calibration corrects the calorimeter response to the true particle-level jet energy [80, 81], where correction factors are obtained from simulation and then refined and validated using data. Corrections for in-time and out-of-time pile-up are also applied. Jets are required to have $|\eta| < 2.5$ and $p_T > 20 \text{ GeV}$ and a “jet vertex fraction” (JVF) larger than 0.5, if $p_T < 50 \text{ GeV}$. The JVF is the p_T -weighted fraction of the tracks in the jet that are associated with the primary vertex. Requiring large JVF values suppresses jets from a different interaction in the same beam bunch crossing. Events containing jets failing to satisfy the quality criteria described in ref. [80] are rejected to suppress events with large calorimeter noise and non-collision backgrounds.

Jets are identified as originating from b -quarks (referred to as b -tagged), using a multivariate technique based on quantities related to reconstructed secondary vertices. The chosen working point of the b -tagging algorithm [82] correctly identifies b -quark jets in simulated $t\bar{t}$ samples with an efficiency of 80%, with a light-flavour jet misidentification probability of about 4%.

Hadronically decaying τ leptons (τ_{had}) are reconstructed using jets described above with $p_T > 10 \text{ GeV}$ and $|\eta| < 2.47$. The τ_{had} reconstruction algorithm uses the electromagnetic and hadronic cluster shapes in the calorimeters, as well as information about the tracks within $\Delta R = 0.2$ of the seed jet. Discriminating track and cluster variables are used within a boosted decision tree algorithm (BDT) to optimise τ_{had} identification. Electrons misidentified as τ_{had} candidates are vetoed using transition radiation and calorimeter information. The τ_{had} candidates are corrected to the τ energy scale [83] using an η - and p_T -dependent calibration. The τ_{had} candidates are required to have one or three associated tracks (prongs) as τ leptons predominantly decay to either one or three charged pions, together with a neutrino and often additional neutral pions. The τ_{had} candidates are also required to have $p_T > 20 \text{ GeV}$ and have unit total charge.

The missing transverse momentum, \vec{p}_T^{miss} (and its magnitude E_T^{miss}), is the negative vector sum of the transverse momenta of all $p_T > 10 \text{ GeV}$ muons, $p_T > 10 \text{ GeV}$ electrons,

$p_T > 10$ GeV photons, $p_T > 20$ GeV jets, and calibrated calorimeter energy clusters with $|\eta| < 4.9$ not associated with these objects. Hadronically decaying τ leptons are included in the \vec{p}_T^{miss} calculation as jets. Clusters associated with electrons, photons and jets are calibrated to the scale of the corresponding objects. Calorimeter clusters not associated with these objects are calibrated using both calorimeter and tracker information [84]. For jets, the calibration includes the pile-up correction described above, whilst the jet vertex fraction requirement is not considered when selecting jet candidates.

In this analysis, “tagged” leptons are candidate leptons separated from each other and from jets in the following order:

1. if two electron candidates are reconstructed with $\Delta R < 0.1$, the lower energy candidate is discarded to avoid double counting.
2. jets within $\Delta R = 0.2$ of an electron candidate, and τ_{had} candidates within $\Delta R = 0.2$ of an electron or muon, are rejected to avoid double counting.
3. electron and muon candidates are rejected if found within $\Delta R = 0.4$ of a jet to suppress semileptonic decays of c - and b -hadrons.
4. to reject bremsstrahlung, close-by electron and muon candidates are both rejected if found within $\Delta R = 0.01$ (0.05 for close-by muon pairs).
5. jets found within $\Delta R = 0.2$ of a “signal” τ lepton (see below) are rejected, to avoid double counting.

Finally, to suppress low mass resonances, if tagged electrons and muons form a same-flavour opposite-sign (SFOS) pair with $m_{\text{SFOS}} < 12$ GeV, both leptons in the pair are rejected.

Tagged leptons satisfying additional identification criteria are called “signal” leptons. Signal τ leptons must satisfy “medium” identification criteria [85]. Signal electrons (muons) are tagged electrons (muons) for which the scalar sum of the transverse momenta of tracks within a cone of $\Delta R = 0.3$ around the lepton candidate is less than 16% (12%) of the lepton p_T . Tracks used for the electron (muon) isolation requirement defined above are those which have $p_T > 0.4$ (1.0) GeV and $|z_0| < 2$ mm with respect to the primary vertex of the event. Tracks of the leptons themselves as well as tracks closer in z_0 to another vertex (that is not the primary vertex) are not included. The isolation requirements are imposed to reduce the contributions from semileptonic decays of hadrons. Signal electrons must also satisfy “tight” identification criteria [77] (modified for 2012 data conditions) and the sum of the extra transverse energy deposits in the calorimeter (corrected for pile-up effects) within a cone of $\Delta R = 0.3$ around the electron candidate must be less than 18% of the electron p_T . To further suppress electrons and muons originating from secondary vertices, the d_0 normalised to its uncertainty is required to be small, with $|d_0|/\sigma(d_0) < 5(3)$, and $|z_0 \sin \theta| < 0.4$ mm (1 mm) for electrons (muons).

6 Event selection

Events are required to have exactly three tagged leptons, passing signal lepton requirements and separated from each other by $\Delta R > 0.3$. At least one electron or muon is required

Table 2. The triggers used in the analysis and the p_T threshold used, ensuring that the lepton(s) triggering the event are in the plateau region of the trigger efficiency. Muons are triggered within a restricted range of $|\eta| < 2.4$.

Trigger	p_T threshold [GeV]
Single Isolated e	25
Single Isolated μ	25
Double e	14,14 25,10
Double μ	14,14 18,10
Combined $e\mu$	14(e),10(μ) 18(μ),10(e)

among the three leptons. The signal electrons and muons in the events must have fired at least one of the single- or double-lepton triggers and satisfied the corresponding p_T -threshold requirements shown in table 2. The p_T thresholds are chosen such that the overall trigger efficiency with respect to the selected events is in excess of 90%, and is independent of the lepton transverse momenta within uncertainties. The same requirements are applied to the MC-simulated events. Events are further required not to contain any b -tagged jets to suppress contributions from top-quark production.

In the following, signal electrons and muons are labelled as ℓ or ℓ' where the flavour of ℓ and ℓ' is assumed to be different. Signal τ_{had} are referred to as τ . Five main signal regions are defined according to the flavour and charge of the leptons, as shown in table 3, and are labelled by the number of τ leptons selected:

SR0 τ a ($\ell^+\ell^-\ell$, $\ell^+\ell^-\ell'$) – a signal region composed of 20 disjoint bins defined in table 4 is optimised for maximum sensitivity to the $\tilde{\ell}_L$ -mediated and WZ -mediated scenarios. SR0 τ a also offers sensitivity to the Wh -mediated scenario. This signal region requires a pair of SFOS leptons among the three leptons and has five slices in m_{SFOS} (defined

Table 3. Summary of the selection requirements for the signal regions. The index of the signal region corresponds to the number of required τ leptons. The SR0 τ a bin definitions are shown in table 4. Energies, momenta and masses are given in units of GeV. The signal models targeted by the selection requirements are also shown.

Signal region	SR0 τ a	SR0 τ b	SR1 τ	SR2 τ a	SR2 τ b
Flavour/sign	$\ell^+\ell^-\ell$, $\ell^+\ell^-\ell'$	$\ell^\pm\ell^\pm\ell'^\mp$	$\tau^\pm\ell^\mp\ell'^\mp$, $\tau^\pm\ell^\mp\ell'^\mp$	$\tau\tau\ell$	$\tau^+\tau^-\ell$
b -tagged jet	veto	veto	veto	veto	veto
E_T^{miss}	binned	> 50	> 50	> 50	> 60
Other	m_{SFOS} binned m_T binned	$p_T^{3^{\text{rd}}\ell} > 20$ $\Delta\phi_{\ell\ell'}^{\text{min}} \leq 1.0$	$p_T^{2^{\text{nd}}\ell} > 30$ $\sum p_T^\ell > 70$ $m_{\ell\tau} < 120$ $m_{ee} Z$ veto	$m_{T2}^{\text{max}} > 100$	$\sum p_T^\tau > 110$ $70 < m_{\tau\tau} < 120$
Target model	$\tilde{\ell}, WZ$ -mediated	Wh -mediated	Wh -mediated	$\tilde{\tau}_L$ -mediated	Wh -mediated

as the invariant mass of the SFOS lepton pair closest to the Z boson mass). Each m_{SFOS} slice is further divided into four bins using $E_{\text{T}}^{\text{miss}}$ and m_{T} selections (see table 4), where m_{T} is the transverse mass formed using the $E_{\text{T}}^{\text{miss}}$ and the lepton not forming the SFOS lepton pair with mass closest to the Z boson mass, $m_{\text{T}}(\vec{p}_{\text{T}}^{\ell}, \vec{p}_{\text{T}}^{\text{miss}}) = \sqrt{2p_{\text{T}}^{\ell}E_{\text{T}}^{\text{miss}} - 2\vec{p}_{\text{T}}^{\ell} \cdot \vec{p}_{\text{T}}^{\text{miss}}}$. Events with tripleton mass, $m_{3\ell}$, close to the Z boson mass ($|m_{3\ell} - m_Z| < 10$ GeV) are vetoed in some bins with low $E_{\text{T}}^{\text{miss}}$ and low m_{T} to suppress contributions from Z boson decays with converted photons from final-state radiation. The WZ and $t\bar{t}$ backgrounds generally dominate the SR0 τ a bins in varying proportions, with WZ mainly dominating the bins for which m_{SFOS} is in the 81.2 – 101.2 GeV range.

SR0 τ b ($\ell^{\pm}\ell^{\pm}\ell'^{\mp}$) – optimised for maximum sensitivity to the Wh -mediated scenario, this signal region vetoes SFOS lepton pairs among the three leptons to effectively suppress the WZ background. Requirements on $E_{\text{T}}^{\text{miss}}$, lepton p_{T} and the minimum $\Delta\phi$ between two opposite-sign (OS) leptons, $\Delta\phi_{\ell\ell'}^{\text{min}}$, are used to reduce the backgrounds. The remaining dominant processes are $t\bar{t}$ and VVV production.

SR1 τ ($\tau^{\pm}\ell^{\mp}\ell^{\mp}$, $\tau^{\pm}\ell^{\mp}\ell'^{\mp}$) – a signal region requiring one τ and two same sign (SS) electrons or muons ($e^{\pm}e^{\pm}$, $e^{\pm}\mu^{\pm}$, $\mu^{\pm}\mu^{\pm}$) is optimised for maximum sensitivity to the Wh -mediated scenario. To increase the sensitivity to the $h \rightarrow \tau\tau$ decay, $m_{\ell\tau}$ is required to be less than 120 GeV, where $m_{\ell\tau}$ is obtained using the ℓ and τ forming the pair closest to the Higgs boson mass of 125 GeV. Electron pairs with mass consistent with a Z boson ($m_{ee} = 81.2\text{--}101.2$ GeV) are vetoed to suppress events in which an electron’s charge is assigned the wrong sign. After requirements on lepton p_{T} , the diboson and $t\bar{t}$ processes dominate the background.

SR2 τ a ($\tau\tau\ell$) – this signal region is optimised for maximum sensitivity to the $\tilde{\ell}_L$ -mediated scenario and also offers some sensitivity to the $\tilde{\ell}_L$ -mediated scenario. It selects events with high $E_{\text{T}}^{\text{miss}}$ and high “stransverse mass” $m_{\text{T}2}^{\text{max}}$ [86, 87]. The stransverse mass is calculated as $m_{\text{T}2}^{\text{max}} = \min_{\vec{q}_{\text{T}}} [\max(m_{\text{T}}(\vec{p}_{\text{T},1}, \vec{q}_{\text{T}}), m_{\text{T}}(\vec{p}_{\text{T},2}, \vec{p}_{\text{T}}^{\text{miss}} - \vec{q}_{\text{T}}))]$, where $\vec{p}_{\text{T},1}$ and $\vec{p}_{\text{T},2}$ are the transverse momenta of the two leptons yielding the largest transverse mass, and \vec{q}_{T} is a transverse vector that minimises the larger of the two transverse masses m_{T} . The dominant background of this signal region is $t\bar{t}$ production.

SR2 τ b ($\tau^{+}\tau^{-}\ell$) – this signal region is optimised for maximum sensitivity to the Wh -mediated scenario and requires two OS τ leptons to target the $h \rightarrow \tau\tau$ decay. Requirements on the p_{T}^{τ} and $E_{\text{T}}^{\text{miss}}$ provide background suppression and the $\tau\tau$ invariant mass $m_{\tau\tau}$ is required to be consistent with that resulting from a Higgs boson decay (and lower than 125 GeV due to escaping neutrinos). Diboson and $t\bar{t}$ processes survive the SR2 τ b selection.

All signal regions are disjoint, with the exception of SR2 τ a and SR2 τ b.

Table 4. Summary of the bins in m_{SFOS} , m_{T} , and $E_{\text{T}}^{\text{miss}}$ for SR0 τ a. All dimensionful values are given in units of GeV.

SR0 τ a bin	m_{SFOS}	m_{T}	$E_{\text{T}}^{\text{miss}}$	3 ℓ Z veto
1	12–40	0–80	50–90	no
2	12–40	0–80	> 90	no
3	12–40	> 80	50–75	no
4	12–40	> 80	> 75	no
5	40–60	0–80	50–75	yes
6	40–60	0–80	> 75	no
7	40–60	> 80	50–135	no
8	40–60	> 80	> 135	no
9	60–81.2	0–80	50–75	yes
10	60–81.2	> 80	50–75	no
11	60–81.2	0–110	> 75	no
12	60–81.2	> 110	> 75	no
13	81.2–101.2	0–110	50–90	yes
14	81.2–101.2	0–110	> 90	no
15	81.2–101.2	> 110	50–135	no
16	81.2–101.2	> 110	> 135	no
17	> 101.2	0–180	50–210	no
18	> 101.2	> 180	50–210	no
19	> 101.2	0–120	> 210	no
20	> 101.2	> 120	> 210	no

7 Standard Model background estimation

Several SM processes lead to events with three signal leptons. Lepton candidates can be classified into three main types, depending on their origin: “real” leptons are prompt and isolated; “fake” leptons can originate from a misidentified light-flavour quark or gluon jet (referred to as “light flavour”); “non-prompt” leptons can originate from a semileptonic decay of a heavy-flavour quark, or an electron from a photon conversion. The SM background processes are classified into “irreducible” background if they lead to events with three or more real leptons, or into “reducible” background if the event has at least one fake or non-prompt lepton. The predictions for irreducible and reducible backgrounds are tested in validation regions (section 7.4).

7.1 Irreducible background processes

Irreducible processes include diboson (WZ and ZZ), VVV , $t\bar{t}V$, tZ and Higgs boson production. The irreducible background contributions are determined using the corresponding MC samples, for which b -tagged jet selection efficiencies and misidentification probabilities, lepton efficiencies, as well as the energy and momentum measurements of leptons and jets are corrected to account for differences with respect to the data.

7.2 Reducible background processes

Reducible processes include single- and pair-production of top quarks, WW production and single W or Z boson produced in association with jets or photons. In signal regions with

fewer than two τ leptons, the dominant reducible background component is $t\bar{t}$, followed by Z +jets, whereas for signal regions with two τ leptons, the dominant component is W +jets. The reducible background is estimated using a “matrix method” similar to that described in ref. [88] and which was previously used in ref. [17].

In this implementation of the matrix method, the highest- p_T signal electron or muon is taken to be real. Simulation studies show that this is a valid assumption in >95% of three-signal-lepton events. The number of observed events with one or two fake or non-prompt leptons is then extracted from a system of linear equations relating the number of events with two additional signal or tagged leptons to the number of events with two additional candidates that are either real, fake or non-prompt. The coefficients of the linear equations are functions of the real-lepton identification efficiencies and of the fake and non-prompt lepton misidentification probabilities, both defined as a fraction of the corresponding tagged leptons passing the signal lepton requirements.

The real-lepton identification efficiencies are obtained from MC simulation in the signal or validation region under consideration to account for detailed kinematic dependencies and are multiplied by correction factors to account for potential differences with respect to the data. The correction factors are obtained from a control region rich in $Z \rightarrow e^+e^-$ and $Z \rightarrow \mu^+\mu^-$ decays and defined with one signal and one tagged lepton, forming a SFOS pair with $|m_{\text{SFOS}} - m_Z| < 10$ GeV. The real-lepton efficiency correction factors are found to be 0.998 ± 0.013 and 0.996 ± 0.001 for electrons and muons respectively, where the uncertainties are statistical.

The fake and non-prompt lepton misidentification probabilities are calculated as the weighted averages of the corrected, type- and process-dependent, misidentification probabilities defined below according to their relative contributions in a given signal or validation region. The type- and process-dependent misidentification probabilities for each relevant fake and non-prompt lepton type (heavy flavour, light flavour or conversion) and for each reducible background process are obtained using simulated events with one signal and two tagged leptons and parameterised with the lepton p_T and η . These misidentification probabilities are then corrected using the ratio (“correction factor”) of the misidentification probability in data to that in simulation obtained from dedicated control samples. The correction factors are assumed to be independent of selected regions and any potential composition or kinematic differences. For non-prompt electrons and muons from heavy-flavour quark decays, the correction factor is measured in a $b\bar{b}$ -dominated control sample. This is defined by selecting events with only one b -tagged jet (containing a muon candidate) and a tagged lepton, for which the misidentification probability is measured. Contaminating backgrounds leading to the production of real leptons from W decays include top-quark pair-production and W bosons produced in association with b -tagged jets. A requirement that $E_T^{\text{miss}} < 60$ GeV suppresses both the $t\bar{t}$ and the W contamination, and requiring $m_T < 50$ GeV (constructed using the tagged lepton) further reduces the W background. The remaining ($\sim 1\%$ level) background is subtracted from data using MC predictions. The heavy-flavour correction factor is found to be 0.74 ± 0.04 (0.89 ± 0.03) for electrons (muons), where the uncertainties are statistical.

Fake τ leptons predominantly originate from light-flavour quark jets. The correspond-

ing correction factor is measured in a W +jets-dominated control sample, where events with one signal muon with $p_T > 25$ GeV and one tagged τ are selected. The muon and τ must be well separated from all other leptons and jets in the event. To suppress $Z \rightarrow \tau\tau$ contributions, $m_T^\mu > 60$ GeV and $\cos \Delta\phi(\vec{p}_T^{\text{miss}}, \vec{p}_T^\mu) + \cos \Delta\phi(\vec{p}_T^{\text{miss}}, \vec{p}_T^\tau) < -0.15$ are imposed. Finally, b -tagged jets are vetoed to suppress heavy-flavour contributions. The light-flavour correction factor decreases from 0.9 to 0.6 (1.0 to 0.6) as the p_T increases from 20 GeV to 150 GeV for one-prong (three-prong) τ decays.

The correction factor for the conversion candidates is determined in events with a converted photon radiated from a muon in $Z \rightarrow \mu\mu$ decays. These are selected by requiring two oppositely charged signal muons and one tagged electron, assumed to originate from the converted photon, such that $|m_{\mu\mu e} - m_Z| < 10$ GeV. The conversion correction factor for electrons is 1.14 ± 0.12 , where the uncertainty is statistical, and is independent of electron p_T and η .

7.3 Systematic uncertainties

Several sources of systematic uncertainties are considered for the SM background estimates and signal yield predictions. The systematic uncertainties affecting the simulation-based estimates (the yield of the irreducible background, the cross-section-weighted misidentification probabilities, and the signal yield) include the theoretical cross-section uncertainties due to the choice of renormalisation and factorisation scales and PDFs, the acceptance uncertainty due to PDFs, the choice of MC generator, the uncertainty on the luminosity (2.8% [89]), the uncertainty due to the jet energy scale, jet energy resolution, lepton energy scale, lepton energy resolution and lepton identification efficiency, the uncertainty on the E_T^{miss} from energy deposits not associated with reconstructed objects, and the uncertainty due to b -tagging efficiency and mistag probability. The systematic uncertainty associated with the simulation of pile-up is also taken into account. An uncertainty is applied to MC samples to cover differences in efficiency seen between the trigger in data and the MC trigger simulation.

The theoretical cross-section uncertainties for the irreducible backgrounds used in this analysis are 30% for $t\bar{t}V$ [51, 52], 50% for tZ , 5% for ZZ , 7% for WZ and 100% for the triboson samples. The ATLAS WZ and ZZ cross-section measurements [90, 91] are in agreement with the MCFM predictions used here. For the Higgs boson samples, 20% uncertainty is used for VH and vector-boson-fusion production, while 100% uncertainty is assigned to $t\bar{t}H$ and Higgs boson production via gluon fusion [49]. The uncertainties on tZ , tribosons, $t\bar{t}H$ and Higgs boson production via gluon fusion are assumed to be large to account for uncertainties on the acceptance, while the inclusive cross-sections are known to better precision. The uncertainty on the WZ and ZZ acceptance due to the choice of MC generator, parton showering and scales is determined by comparing estimates from POWHEG and aMC@NLO, while those for $t\bar{t}V$ are determined by comparing ALPGEN and MADGRAPH estimates.

The uncertainty on the reducible background includes the MC uncertainty on the weights for the misidentification probabilities from the sources listed in section 7.2 (2–14%) and the uncertainty due to the dependence of the misidentification probability on

Table 5. Summary of the selection requirements for the validation regions. Energies, momenta and masses are given in units of GeV.

Region name	N(ℓ)	N(τ)	Flavour/sign	Z boson	E_T^{miss}	N(b -tagged jets)	Target process
VR0 τ noZa	3	0	$\ell^+\ell^-\ell, \ell^+\ell^-\ell'$	$m_{\text{SFOS}} \& m_{3\ell}$ veto	35–50	–	$WZ^*, Z^*Z^*, Z^*+\text{jets}$
VR0 τ Za	3	0	$\ell^+\ell^-\ell, \ell^+\ell^-\ell'$	request	35–50	–	$WZ, Z+\text{jets}$
VR0 τ noZb	3	0	$\ell^+\ell^-\ell, \ell^+\ell^-\ell'$	$m_{\text{SFOS}} \& m_{3\ell}$ veto	> 50	1	$t\bar{t}$
VR0 τ Zb	3	0	$\ell^+\ell^-\ell, \ell^+\ell^-\ell'$	request	> 50	1	WZ
VR0 τ b	3	0	$\ell^+\ell^-\ell, \ell^+\ell^-\ell'$	binned	binned	1	$WZ, t\bar{t}$
VR1 τ a	2	1	$\tau^\pm\ell^\mp\ell^\mp, \tau^\pm\ell^\mp\ell'^\mp$	–	35–50	–	$WZ, Z+\text{jets}$
VR1 τ b	2	1	$\tau^\pm\ell^\mp\ell^\mp, \tau^\pm\ell^\mp\ell'^\mp$	–	> 50	1	$t\bar{t}$
VR2 τ a	1	2	$\tau\tau\ell$	–	35–50	–	$W+\text{jets}, Z+\text{jets}$
VR2 τ b	1	2	$\tau\tau\ell$	–	> 50	1	$t\bar{t}$

E_T^{miss} (0–7%), m_T (1–7%), $m_{\ell\ell}$ (0–18%), SFOS selection/veto (0–5%) and η (1–5%). Also included in the uncertainty on the reducible background is the uncertainty on the correction factors for the misidentification probability, the statistical uncertainty on the data events used to apply the matrix equation and the statistical uncertainty from the misidentification probability measured in simulation.

7.4 Background modelling validation

The background predictions are tested in validation regions that are defined to be adjacent to, yet disjoint from, the signal regions. For each τ multiplicity considered, validation regions are defined with either low- E_T^{miss} (“a” regions) or high- E_T^{miss} + b -tagged jet (“b” regions) to target different background processes. The definition of the regions and the targeted processes are shown in table 5. In the validation region requiring no τ leptons, both the Z -veto and Z -request regions are tested in the low- E_T^{miss} and high- E_T^{miss} + b -tagged jet regions. To validate the binned signal region SR0 τ a, an orthogonal validation region (VR0 τ b) is defined with the same binning as shown in table 4 and a b -tagged jet requirement.

Table 6. Expected numbers of SM background events and observed numbers of data events in selected validation regions, as defined in table 5. The binned validation region VR0 τ b is displayed in figure 2. Statistical and systematic uncertainties are included (as described in section 7.3). CL_b values are given.

Sample	VR0 τ noZa	VR0 τ Za	VR0 τ noZb	VR0 τ Zb	VR1 τ a	VR1 τ b	VR2 τ a	VR2 τ b
WZ	91 ± 12	471 ± 47	$10.5^{+1.8}_{-2.0}$	58 ± 7	14.6 ± 1.9	1.99 ± 0.35	$14.3^{+2.4}_{-2.5}$	1.9 ± 0.4
ZZ	19 ± 4	48 ± 7	0.62 ± 0.12	2.6 ± 0.4	$1.76^{+0.29}_{-0.28}$	0.138 ± 0.028	1.8 ± 0.4	0.12 ± 0.04
$t\bar{t}V + tZ$	3.2 ± 1.0	$10.1^{+2.3}_{-2.2}$	9.5 ± 3.1	18 ± 4	0.9 ± 0.9	2.8 ± 1.3	1.0 ± 0.7	1.7 ± 0.7
VVV	1.9 ± 1.9	0.7 ± 0.7	$0.35^{+0.36}_{-0.35}$	0.18 ± 0.18	0.4 ± 0.4	0.08 ± 0.08	0.12 ± 0.12	$0.06^{+0.07}_{-0.06}$
Higgs	2.7 ± 1.3	2.7 ± 1.5	1.5 ± 1.0	0.71 ± 0.29	0.57 ± 0.34	0.5 ± 0.5	0.6 ± 0.4	0.5 ± 0.5
Reducible	73^{+20}_{-17}	261 ± 70	47^{+15}_{-13}	19 ± 5	71 ± 9	22.7 ± 2.8	630^{+9}_{-12}	162^{+6}_{-8}
Total SM	191^{+24}_{-22}	794 ± 86	69^{+15}_{-14}	98 ± 10	89^{+10}_{-9}	28.2 ± 3.2	648^{+10}_{-13}	166^{+6}_{-8}
Data	228	792	79	110	82	26	656	158
CL_b	0.90	0.49	0.72	0.79	0.30	0.37	0.61	0.30

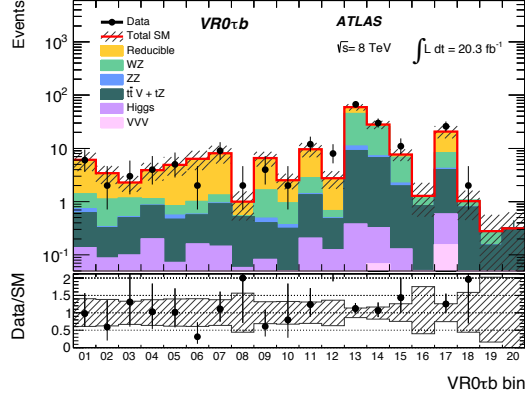


Figure 2. Number of expected and observed events in the validation region VR0 τ b. Also shown are the respective contributions of the various background processes as described in the legend. The uncertainty band includes both the statistical and systematic uncertainties on the SM prediction.

In the validation regions, the observed data count and SM expectations are in good agreement within statistical and systematic uncertainties, as shown in table 6 and figure 2. The CL_b value [92], using a profile likelihood ratio as a test statistic [93], verifies the compatibility of the observation with the background prediction. Values of CL_b above (below) 0.5 indicate the observed level of agreement above (below) the expected yield. The m_T distributions in VR0 τ noZa and VR0 τ Za along with the $m_{\ell\tau}$ distribution in VR1 τ a and m_{T2}^{\max} distribution in VR2 τ a are shown in figure 3, while the E_T^{miss} distributions in the high- E_T^{miss} + b -tagged jet validation regions are presented in figure 4.

While the results from the validation regions are not used to derive correction factors for the background, potential signal contamination is assessed. It is found to be at the sub-percent level for most of the SUSY scenarios considered except for some characterised by low chargino mass. These scenarios would, however, lead to a detectable signal in the signal regions.

8 Results and interpretations

The observed number of events in each signal region is shown in tables 7 and 8 along with the background expectations and uncertainties. The uncertainties include both the statistical and systematic components described in section 7.3. A summary of the dominant systematic uncertainties in each signal region is given in table 9.

Figure 5 shows the SM expectations and the observations in data in the individual SR0 τ a bins as well as the distribution of E_T^{miss} , m_T and m_{SFOS} in the combination of all SR0 τ a regions. For illustration, the distributions are also shown for the WZ -mediated and $\tilde{\ell}_L$ -mediated simplified models.

Figure 6 shows the distributions of the quantities $\Delta\phi_{\ell\ell'}^{\min}$, E_T^{miss} , m_{T2}^{\max} and $m_{\tau\tau}$ in the SR0 τ b, SR1 τ , SR2 τ a and SR2 τ b regions respectively, prior to the requirements on these variables. Also shown are the distributions of these quantities for signal hypotheses from the $\tilde{\tau}_L$ -mediated and Wh -mediated simplified models.

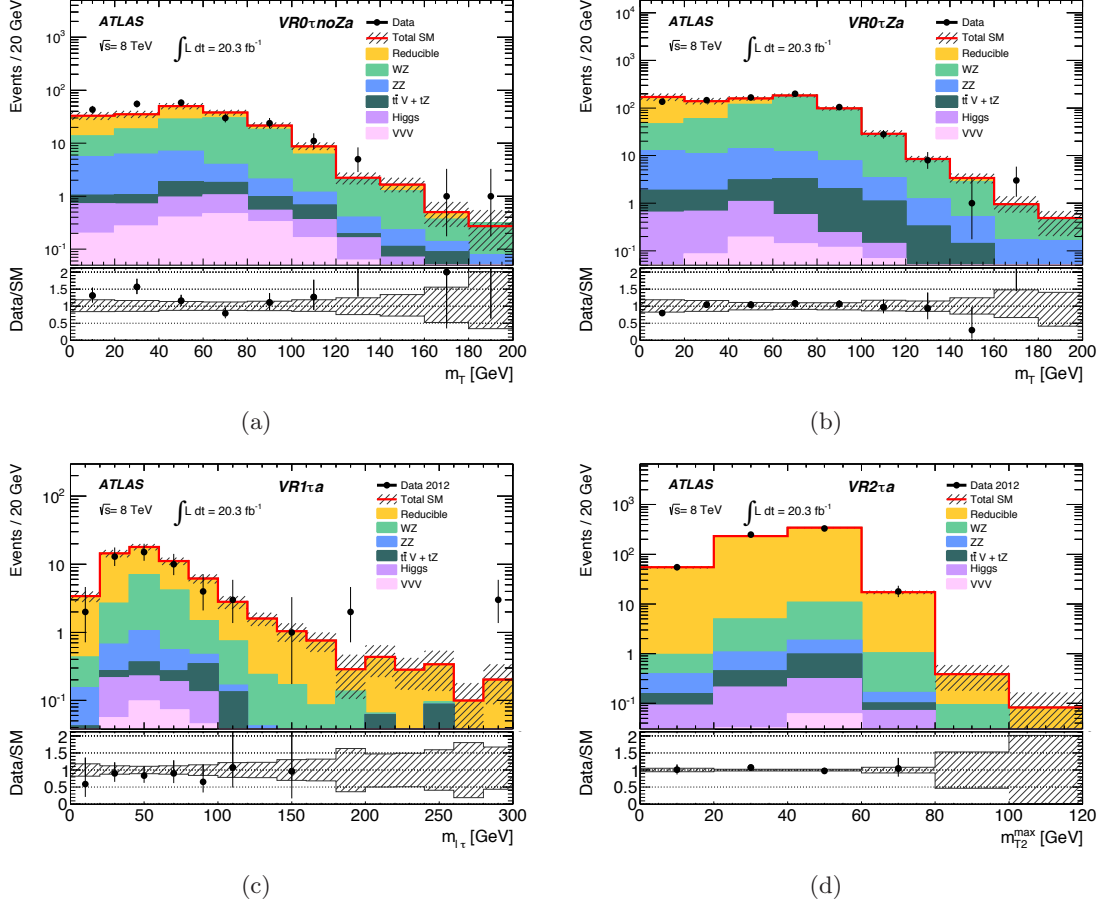


Figure 3. For events in the low- E_T^{miss} validation regions, the m_T distribution in (a) VR0 τ noZa, (b) VR0 τ Za, (c) the $m_{\ell\tau}$ distribution in VR1 τ a and (d) the m_{T2}^{max} distribution in VR2 τ a, see text for details. Also shown are the respective contributions of the various background processes as described in the legend. The uncertainty band includes both the statistical and systematic uncertainties on the SM prediction. The last bin in each distribution includes the overflow.

The number of observed events is consistent with the SM expectation in all signal regions, within uncertainties. The one-sided p_0 -value is calculated to quantify the probability of the SM background alone to fluctuate to the observed number of events or higher (shown in table 7 and table 8), and is truncated to 0.5 for $p_0 > 0.5$. Upper limits at 95% CL on the expected and observed number of beyond the SM events (N_{exp}^{95} and N_{obs}^{95}) for each signal region are calculated using the CL_s prescription [92] and shown in table 7 and table 8. The profile likelihood ratio is used as a test statistic [93] and sources of systematic uncertainties are treated as nuisance parameters. The p_0 and CL_s values are calculated using pseudo-experiments.

The results obtained are used to derive limits on the simplified and pMSSM models described in section 2. Exclusion limits are calculated by statistically combining results from a number of disjoint signal regions. For the $\tilde{\ell}_L$ -mediated, WZ -mediated and $\tilde{\tau}_L$ -mediated simplified models and for the pMSSM scenarios, SR0 τ a, SR0 τ b, SR1 τ and SR2 τ a are sta-

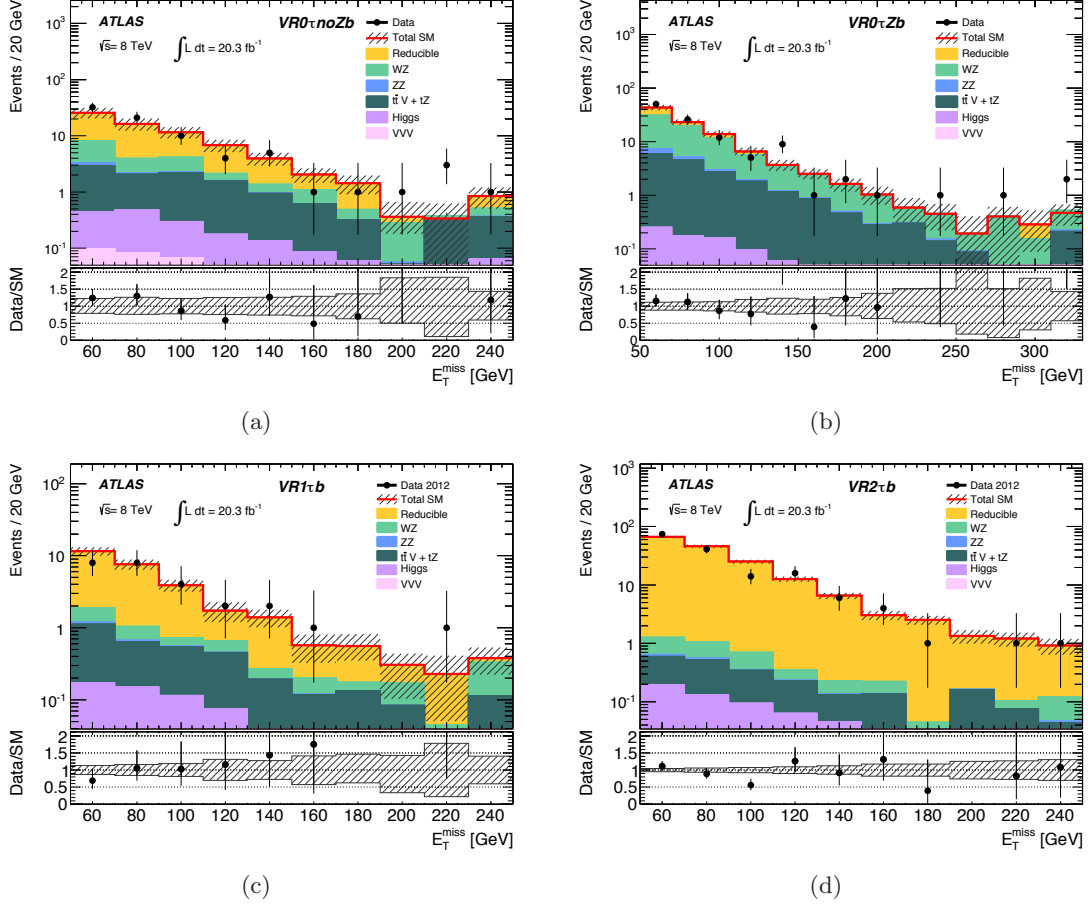


Figure 4. For events in the high- $E_T^{\text{miss}} + b$ -tagged jet validation regions, the E_T^{miss} distribution in (a) VR0 τ noZb, (b) VR0 τ Zb, (c) VR1 τ b and (d) VR2 τ b. Also shown are the respective contributions of the various background processes as described in the legend. The uncertainty band includes both the statistical and systematic uncertainties on the SM prediction. The last bin in each distribution includes the overflow.

tistically combined. For the Wh -mediated simplified model, the statistical combination of SR0 τ a, SR0 τ b, SR1 τ and SR2 τ b is used. All experimental uncertainties are treated as correlated between regions and processes, with the exception of the experimental uncertainties on the reducible background, which are correlated between regions only. Theoretical uncertainties on the irreducible background and signal are treated as correlated between regions, while statistical uncertainties are treated as uncorrelated between regions and processes. The total systematic uncertainty on all SUSY signal processes is in the 10–20% range, where $\sim 7\%$ originates from the uncertainty on the signal cross-section. The uncertainty due to changes in signal acceptance from varying the PDFs and the amount of initial-state radiation is found to be negligible compared to the total systematic uncertainty for the signal scenarios under consideration. For the exclusion limits, the observed and expected 95% CL limits are calculated using pseudo-experiments for each SUSY model point, taking into account the theoretical and experimental uncertainties on the SM background and the

Table 7. Expected numbers of SM background events and observed numbers of data events in the signal regions SR0 τ a-bin01–bin12 for 20.3 fb $^{-1}$. Statistical and systematic uncertainties are included as described in section 7.3. Also shown are the one-sided p_0 -values and the upper limits at 95% CL on the expected and observed number of beyond-the-SM events (N_{exp}^{95} and N_{obs}^{95}) for each signal region, calculated using pseudo-experiments and the CL $_s$ prescription. For p_0 -values below 0.5, the observed number of standard deviations, σ , is also shown in parentheses.

Sample	SR0 τ a-bin01	SR0 τ a-bin02	SR0 τ a-bin03	SR0 τ a-bin04	SR0 τ a-bin05	SR0 τ a-bin06
WZ	$13.2^{+3.4}_{-3.2}$	3.0 ± 1.4	7.8 ± 1.6	$4.5^{+1.1}_{-1.0}$	6.3 ± 1.6	3.7 ± 1.6
ZZ	$1.4^{+0.6}_{-0.5}$	0.12 ± 0.06	0.40 ± 0.14	0.20 ± 0.18	1.5 ± 0.5	$0.25^{+0.14}_{-0.11}$
$t\bar{t}V + tZ$	0.14 ± 0.05	0.07 ± 0.04	$0.04^{+0.05}_{-0.04}$	0.14 ± 0.13	0.11 ± 0.08	$0.047^{+0.022}_{-0.021}$
VVV	0.33 ± 0.33	0.10 ± 0.10	0.19 ± 0.19	0.6 ± 0.6	$0.26^{+0.27}_{-0.26}$	0.24 ± 0.24
Higgs	0.66 ± 0.26	0.15 ± 0.08	0.64 ± 0.22	$0.46^{+0.18}_{-0.17}$	$0.36^{+0.14}_{-0.15}$	$0.33^{+0.13}_{-0.12}$
Reducible	6.7 ± 2.4	0.8 ± 0.4	$1.6^{+0.7}_{-0.6}$	2.7 ± 1.0	$4.3^{+1.6}_{-1.4}$	2.0 ± 0.8
Total SM	23 ± 4	4.2 ± 1.5	10.6 ± 1.8	$8.5^{+1.7}_{-1.6}$	$12.9^{+2.4}_{-2.3}$	$6.6^{+1.9}_{-1.8}$
Data	36	5	9	9	11	13
p_0 (σ)	0.02 (2.16)	0.35 (0.38)	0.50	0.40 (0.26)	0.50	0.03 (1.91)
N_{exp}^{95}	$14.1^{+5.6}_{-3.6}$	$6.2^{+2.5}_{-1.7}$	$8.4^{+3.1}_{-2.3}$	$7.7^{+3.1}_{-2.1}$	$9.0^{+3.6}_{-2.5}$	$8.0^{+3.2}_{-1.9}$
N_{obs}^{95}	26.8	6.9	7.3	8.4	7.9	14.4

Sample	SR0 τ a-bin07	SR0 τ a-bin08	SR0 τ a-bin09	SR0 τ a-bin10	SR0 τ a-bin11	SR0 τ a-bin12
WZ	7.6 ± 1.3	$0.30^{+0.25}_{-0.24}$	$16.2^{+3.2}_{-3.1}$	$13.1^{+2.5}_{-2.6}$	19 ± 4	3.7 ± 1.2
ZZ	$0.55^{+0.16}_{-0.14}$	$0.012^{+0.008}_{-0.007}$	$1.43^{+0.32}_{-0.28}$	$0.60^{+0.12}_{-0.13}$	0.7 ± 1.2	0.14 ± 0.09
$t\bar{t}V + tZ$	$0.04^{+0.15}_{-0.04}$	$0.12^{+0.13}_{-0.12}$	$0.16^{+0.09}_{-0.12}$	0.12 ± 0.10	$0.41^{+0.24}_{-0.22}$	0.12 ± 0.11
VVV	0.9 ± 0.9	$0.13^{+0.14}_{-0.13}$	$0.23^{+0.24}_{-0.23}$	0.4 ± 0.4	0.6 ± 0.6	0.6 ± 0.6
Higgs	$0.98^{+0.29}_{-0.30}$	0.13 ± 0.06	0.32 ± 0.11	$0.22^{+0.10}_{-0.11}$	0.28 ± 0.12	0.12 ± 0.06
Reducible	$4.0^{+1.5}_{-1.4}$	$0.40^{+0.27}_{-0.26}$	$4.1^{+1.3}_{-1.2}$	$1.9^{+0.9}_{-0.8}$	$5.7^{+2.1}_{-1.9}$	$0.9^{+0.5}_{-0.4}$
Total SM	14.1 ± 2.2	1.1 ± 0.4	$22.4^{+3.6}_{-3.4}$	16.4 ± 2.8	27 ± 5	$5.5^{+1.5}_{-1.4}$
Data	15	1	28	24	29	8
p_0 (σ)	0.37 (0.33)	0.50	0.13 (1.12)	0.07 (1.50)	0.39 (0.28)	0.21 (0.82)
N_{exp}^{95}	$9.6^{+3.9}_{-2.5}$	$3.7^{+1.5}_{-0.9}$	$12.7^{+4.9}_{-3.5}$	$11.3^{+4.5}_{-3.1}$	$13.8^{+5.4}_{-3.7}$	$6.9^{+2.9}_{-1.7}$
N_{obs}^{95}	10.8	3.7	18.0	18.3	15.3	9.2

experimental uncertainties on the signal. The impact of the theoretical uncertainties on the signal cross-section is shown for the observed limit and where quoted, limits refer to the -1σ variation on the observed limit.

In the $\tilde{\ell}_L$ -mediated simplified model, $\tilde{\chi}_1^\pm$ and $\tilde{\chi}_2^0$ masses are excluded up to 700 GeV as shown in figure 7(a). The region SR0 τ a-bin20 offers the best sensitivity to scenarios with high $\tilde{\chi}_1^\pm$ and $\tilde{\chi}_2^0$ masses, and the low- m_{SFOS} SR0 τ a bins to the small $m_{\tilde{\chi}_2^0} - m_{\tilde{\chi}_1^0}$ scenarios. In the WZ -mediated simplified model shown in figure 7(b), $\tilde{\chi}_1^\pm$ and $\tilde{\chi}_2^0$ masses are excluded up

Table 8. Expected numbers of SM background events and observed numbers of data events in the signal regions SR0 τ a-bin13–bin20, SR0 τ b, SR1 τ , SR2 τ a and SR2 τ b for 20.3 fb $^{-1}$. Statistical and systematic uncertainties are included as described in section 7.3. Also shown are the one-sided p_0 -values and the upper limits at 95% CL on the expected and observed number of beyond-the-SM events (N_{exp}^{95} and N_{obs}^{95}) for each signal region, calculated using pseudo-experiments and the CL $_s$ prescription. For p_0 -values below 0.5, the observed number of standard deviations, σ , is also shown in parentheses.

Sample	SR0 τ a-bin13	SR0 τ a-bin14	SR0 τ a-bin15	SR0 τ a-bin16	SR0 τ a-bin17	SR0 τ a-bin18
WZ	613 ± 65	207^{+33}_{-32}	58^{+12}_{-13}	$3.9^{+1.6}_{-1.4}$	50^{+7}_{-6}	2.3 ± 1.3
ZZ	29 ± 4	5.5 ± 1.5	$3.5^{+1.1}_{-1.0}$	$0.12^{+0.08}_{-0.07}$	$2.4^{+0.7}_{-0.6}$	0.08 ± 0.04
$t\bar{t}V + tZ$	$2.9^{+0.7}_{-0.6}$	$2.0^{+0.7}_{-0.6}$	$0.67^{+0.29}_{-0.28}$	$0.08^{+0.10}_{-0.08}$	0.8 ± 0.5	$0.15^{+0.16}_{-0.15}$
VVV	1.3 ± 1.3	0.8 ± 0.8	1.0 ± 1.0	0.33 ± 0.33	3.2 ± 3.2	0.5 ± 0.5
Higgs	2.2 ± 0.7	0.98 ± 0.20	0.31 ± 0.11	0.033 ± 0.018	0.95 ± 0.29	0.05 ± 0.04
Reducible	68^{+21}_{-19}	$2.2^{+1.9}_{-2.0}$	1.2 ± 0.6	$0.14^{+0.25}_{-0.14}$	$11.3^{+3.5}_{-3.2}$	0.27 ± 0.20
Total SM	715 ± 70	219 ± 33	65 ± 13	$4.6^{+1.7}_{-1.5}$	69^{+9}_{-8}	3.4 ± 1.4
Data	714	214	63	3	60	1
p_0 (σ)	0.50	0.50	0.50	0.50	0.50	0.50
N_{exp}^{95}	133^{+46}_{-36}	66^{+24}_{-18}	$28.6^{+10.1}_{-7.2}$	$5.9^{+2.6}_{-1.5}$	$21.4^{+8.2}_{-5.6}$	$4.8^{+2.0}_{-1.1}$
N_{obs}^{95}	133	65	27.6	5.2	18.8	3.7

Sample	SR0 τ a-bin19	SR0 τ a-bin20	SR0 τ b	SR1 τ	SR2 τ a	SR2 τ b
WZ	0.9 ± 0.4	0.12 ± 0.11	0.68 ± 0.20	4.6 ± 0.6	$1.51^{+0.35}_{-0.33}$	$2.09^{+0.30}_{-0.31}$
ZZ	0.021 ± 0.019	0.009 ± 0.009	0.028 ± 0.009	0.36 ± 0.08	$0.049^{+0.016}_{-0.014}$	0.135 ± 0.025
$t\bar{t}V + tZ$	$0.0023^{+0.0032}_{-0.0019}$	$0.012^{+0.016}_{-0.012}$	$0.17^{+0.32}_{-0.17}$	$0.16^{+0.18}_{-0.16}$	$0.21^{+0.27}_{-0.21}$	$0.023^{+0.015}_{-0.018}$
VVV	0.08 ± 0.08	$0.07^{+0.08}_{-0.07}$	1.0 ± 1.0	0.5 ± 0.5	0.09 ± 0.09	0.031 ± 0.033
Higgs	0.007 ± 0.006	0.0009 ± 0.0004	0.49 ± 0.17	0.28 ± 0.12	0.021 ± 0.010	0.08 ± 0.04
Reducible	$0.17^{+0.16}_{-0.15}$	$0.08^{+0.11}_{-0.08}$	1.5 ± 0.4	4.3 ± 0.8	5.1 ± 0.7	4.9 ± 0.7
Total SM	1.2 ± 0.4	$0.29^{+0.18}_{-0.17}$	3.8 ± 1.2	10.3 ± 1.2	6.9 ± 0.8	$7.2^{+0.7}_{-0.8}$
Data	0	0	3	13	6	5
p_0 (σ)	0.50	0.50	0.50	0.19 (0.86)	0.50	0.50
N_{exp}^{95}	$3.7^{+1.4}_{-0.7}$	$3.0^{+0.8}_{-0.0}$	$5.6^{+2.2}_{-1.4}$	$8.1^{+3.2}_{-2.2}$	$6.8^{+2.7}_{-1.9}$	$6.7^{+2.8}_{-1.8}$
N_{obs}^{95}	3.0	3.0	5.4	10.9	6.0	5.2

to 345 GeV for massless $\tilde{\chi}_1^0$. The region SR0 τ a-bin16 offers the best sensitivity to scenarios with high $\tilde{\chi}_1^\pm$ and $\tilde{\chi}_2^0$ masses, and SR0 τ a-bin01 to the small $m_{\tilde{\chi}_2^0} - m_{\tilde{\chi}_1^0}$ scenarios. The results in the signal regions lead to a weaker (stronger) observed exclusion than expected for the compressed (high-mass $\tilde{\chi}_1^\pm, \tilde{\chi}_2^0$) scenarios in both the $\tilde{\ell}_L$ -mediated and WZ -mediated simplified models. In the WZ -mediated simplified model, there is a reduced sensitivity to scenarios in the $m_{\tilde{\chi}_2^0} - m_{\tilde{\chi}_1^0} = m_Z$ region as the signal populates regions with high WZ

Table 9. Summary of the dominant systematic uncertainties in the background estimates for each signal region. Uncertainties are quoted relative to the total expected background. For the 20 bins of the SR0 τ a the range of the uncertainties is provided.

	SR0 τ a	SR0 τ b	SR1 τ	SR2 τ a	SR2 τ b
Cross-section	4–25%	37%	9%	3.1%	3.0%
Generator	3.2–35%	11%	3.1%	6%	< 1%
Statistics on irreducible background	0.8–26%	8%	5%	5%	3.1%
Statistics on reducible background	0.4–29%	14%	8%	13%	12%
Electron misidentification probability	0.3–10%	1.3%	< 1%	–	–
Muon misidentification probability	0.1–24%	2.2%	< 1%	–	–
τ misidentification probability	–	–	8%	4%	5%

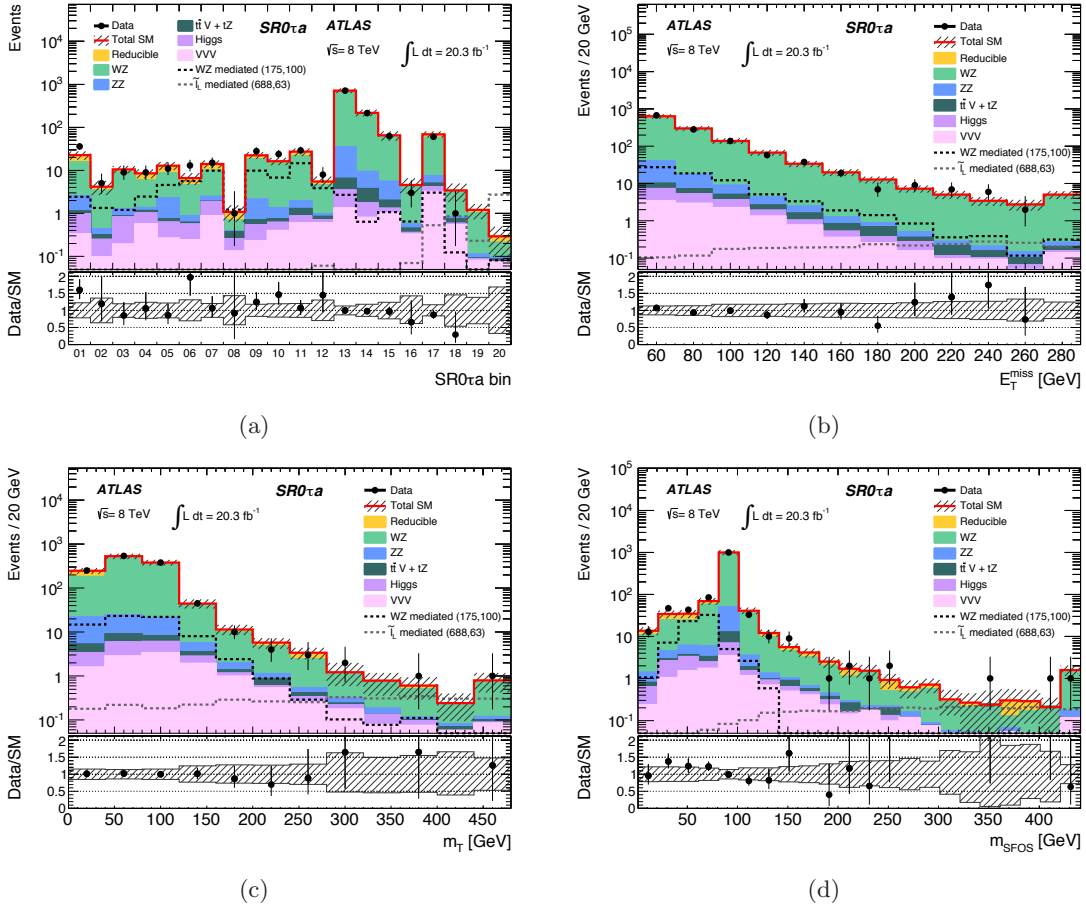


Figure 5. Expected distributions of SM background events and observed data distributions in (a) the binned signal regions SR0 τ a. The distributions of (b) E_T^{miss} , (c) m_T and (d) m_{SFOS} are shown in the summation of all SR0 τ a regions prior to the requirements on these variables. Also shown are the respective contributions of the various background processes as described in the legend. Both the statistical and systematic uncertainties are shown. The last bin in each distribution includes the overflow. For illustration, the distributions of signal hypotheses are also shown.

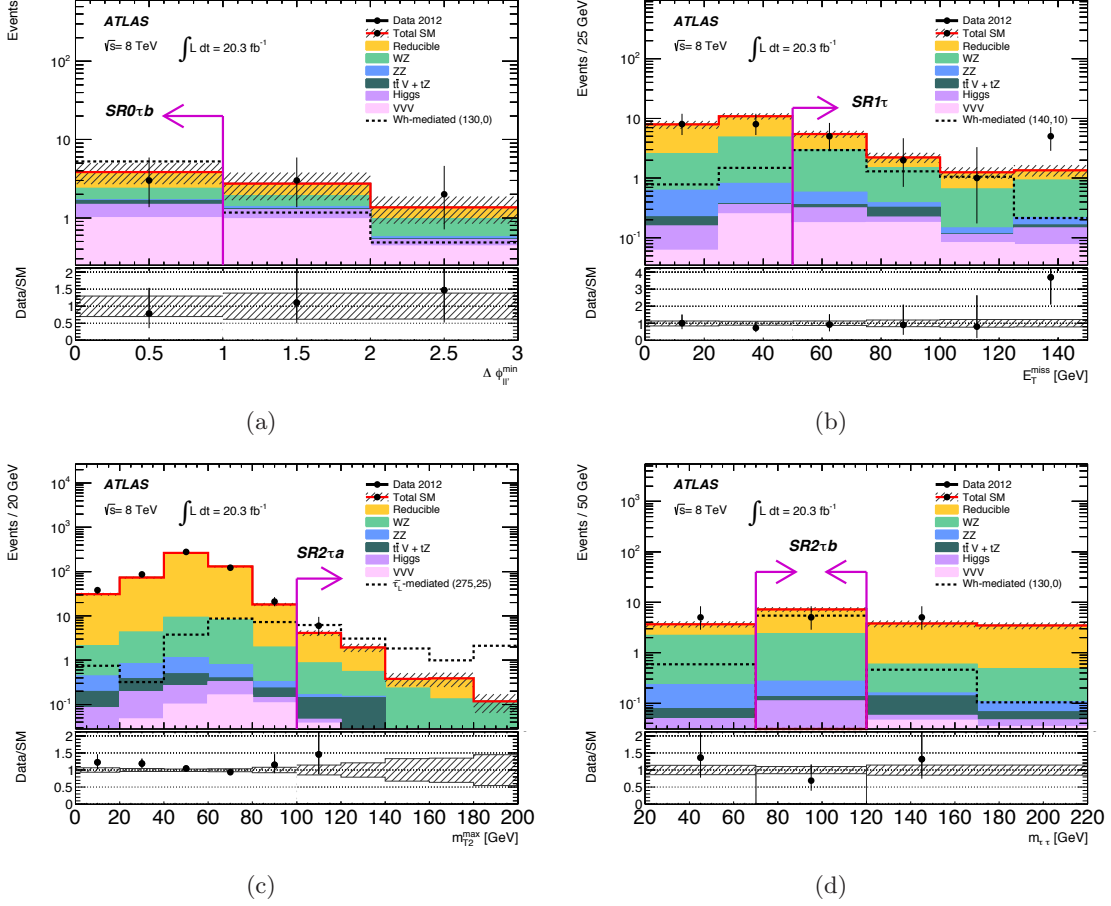


Figure 6. Expected distributions of SM background events and observed data distributions for (a) $\Delta\phi_{\ell\ell'}$, (b) E_T^{miss} , (c) m_{T2}^{max} and (d) $m_{\tau\tau}$ variables in the SR0 τ b, SR1 τ , SR2 τ a and SR2 τ b regions respectively, prior to the requirements on these variables. Arrows indicate the limits on the values of the variables used to define the signal regions. Also shown are the respective contributions of the various background processes as described in the legend. Both the statistical and systematic uncertainties are shown. The last bin in each distribution includes the overflow. The plots also show the distribution for signal hypotheses, where the parentheses following the simplified model denote the mass parameters in GeV as $(m(\tilde{\chi}_1^\pm, \tilde{\chi}_2^0), m(\tilde{\chi}_1^0))$.

background. These limits improve those reported by ATLAS in ref. [17] by ~ 200 GeV.

In the $\tilde{\tau}_L$ -mediated simplified model, $\tilde{\chi}_1^\pm$ and $\tilde{\chi}_2^0$ masses are excluded up to 380 GeV for massless $\tilde{\chi}_1^0$ as shown in figure 7(c). The low m_{SFOS} SR0 τ a bins offer the best sensitivity to the small $m_{\tilde{\chi}_2^0} - m_{\tilde{\chi}_1^0}$ scenarios, and SR2 τ a to the high-mass $\tilde{\chi}_1^\pm, \tilde{\chi}_2^0$ scenarios. The results in the low m_{SFOS} SR0 τ a bins lead to a weaker observed exclusion than expected for the compressed scenarios.

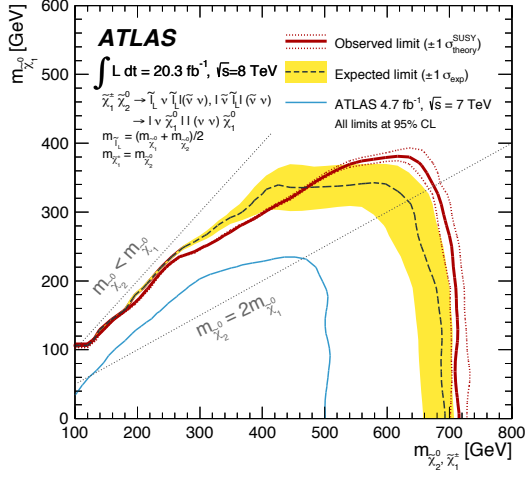
In the Wh -mediated simplified model shown in figure 7(d), $\tilde{\chi}_1^\pm$ and $\tilde{\chi}_2^0$ masses are excluded up to 148 GeV. The regions SR0 τ a, SR0 τ b, SR1 τ and SR2 τ b offer the best sensitivity in this simplified model when statistically combined. The results in some SR0 τ a bins and SR1 τ are responsible for the observed exclusion being slightly weaker than ex-

pected.

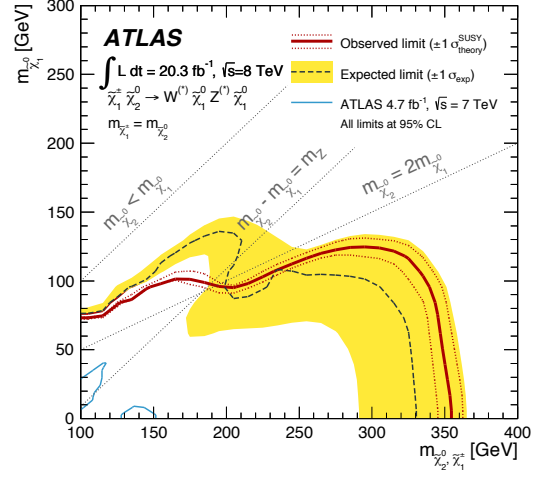
In the pMSSM scenarios shown in figure 8, for a given value of M_1 , the sensitivity for high values of M_2 and μ , and therefore for high values of chargino and heavy neutralino masses, is driven by the decrease of the production cross-section. Due to small $m_{\tilde{\chi}_2^0} - m_{\tilde{\chi}_1^0}$ or $m_{\tilde{\chi}_1^\pm} - m_{\tilde{\chi}_1^0}$, limited sensitivity is found in the regions with $M_1 \sim M_2 \ll \mu$, as seen in figures 8(a–d). In the case of the pMSSM $\tilde{\tau}_R$ scenario, the small mass splittings also reduce the sensitivity in the $M_1 \sim \mu \ll M_2$ region. In the pMSSM $\tilde{\ell}_R$ scenario with $M_1 = 250$ GeV, the $M_2 \gtrsim 250$ GeV and $\mu \gtrsim 250$ GeV region is characterised by small $m_{\tilde{\chi}_1^\pm} - m_{\tilde{\chi}_1^0}$, and due to the results in SR0 τ a-bin01 the observed exclusion region is significantly smaller than that expected. For the pMSSM no $\tilde{\ell}$ scenarios, in the region with $M_2 \gtrsim 200$ GeV and $\mu \gtrsim 200$ GeV the decay mode $\tilde{\chi}_2^0 \rightarrow h\tilde{\chi}_1^0$ is kinematically allowed and reduces the sensitivity.

9 Conclusions

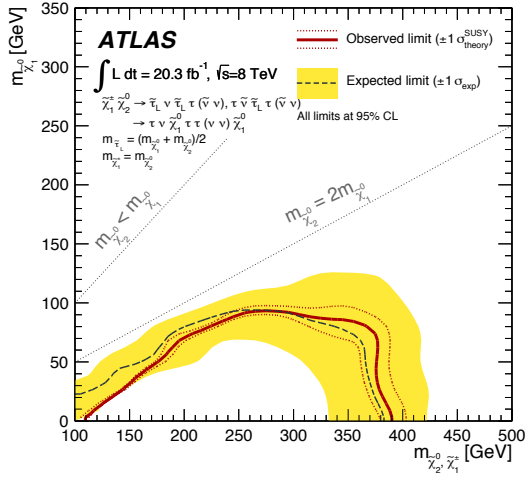
This paper describes a search for the production of charginos and neutralinos decaying into final states with three leptons (e , μ , τ) and missing transverse momentum. The analysis uses 20.3 fb^{-1} of $\sqrt{s} = 8$ TeV proton-proton collision data delivered by the LHC and recorded with the ATLAS detector in 2012. No significant excess of events above SM expectations is found in data. The null result is interpreted in simplified SUSY models and in various pMSSM scenarios. For the simplified SUSY models with intermediate slepton decays, degenerate $\tilde{\chi}_1^\pm$ and $\tilde{\chi}_2^0$ masses up to 700 GeV are excluded for large mass differences with the $\tilde{\chi}_1^0$, while for the simplified SUSY models with gauge boson decays, the exclusion reaches 345 GeV. These limits improve upon the previous ATLAS results in ref. [17] by ~ 200 GeV. For the simplified SUSY models with intermediate staus, degenerate $\tilde{\chi}_1^\pm$ and $\tilde{\chi}_2^0$ masses up to 380 GeV are excluded, while for the simplified SUSY models with intermediate Higgs boson decays, degenerate $\tilde{\chi}_1^\pm$ and $\tilde{\chi}_2^0$ masses up to 148 GeV are excluded.



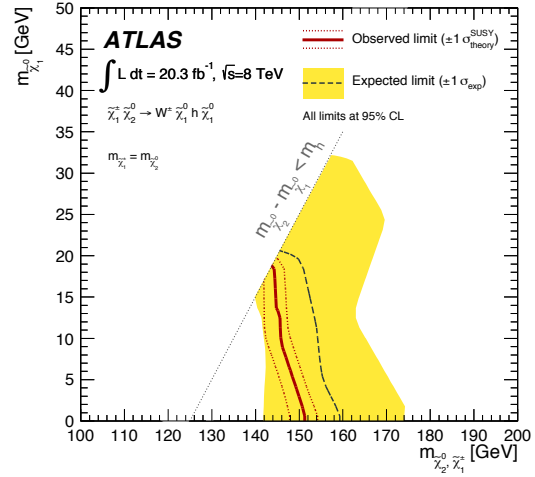
(a) $\tilde{\ell}_L$ -mediated simplified model



(b) WZ -mediated simplified model

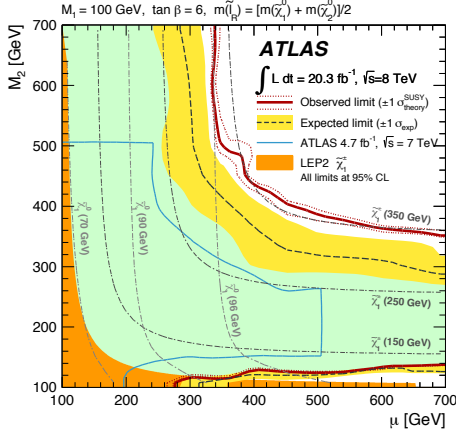


(c) $\tilde{\tau}_L$ -mediated simplified model

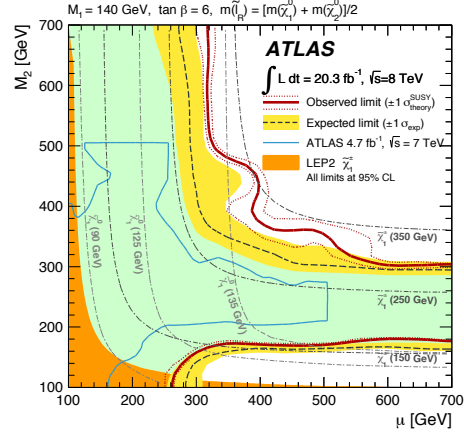


(d) Wh -mediated simplified model

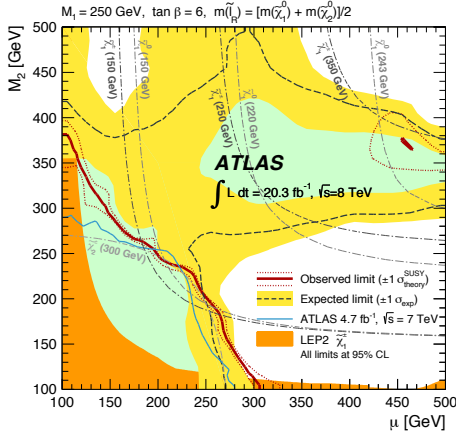
Figure 7. Observed and expected 95% CL exclusion contours for chargino and neutralino production in the (a) $\tilde{\ell}_L$ -mediated, (b) WZ -mediated, (c) $\tilde{\tau}_L$ -mediated and (d) Wh -mediated simplified models. The band around the expected limit shows the $\pm 1\sigma$ variations of the expected limit, including all uncertainties except theoretical uncertainties on the signal cross-section. The dotted lines around the observed limit indicate the sensitivity to $\pm 1\sigma$ variations of these theoretical uncertainties. The blue contours in (a) and (b) correspond to the 7 TeV limits from the ATLAS three-lepton analysis [17]. Linear interpolation is used to account for the discrete nature of the signal grids.



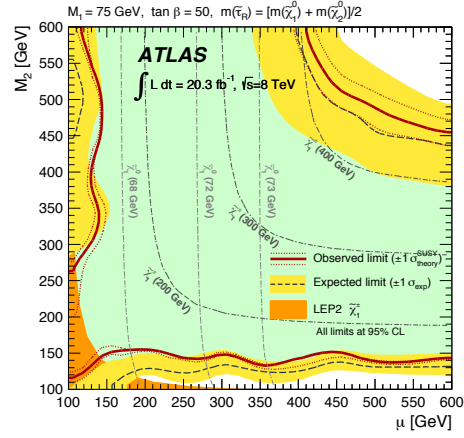
(a) pMSSM $\tilde{\ell}_R$, $M_1=100$ GeV



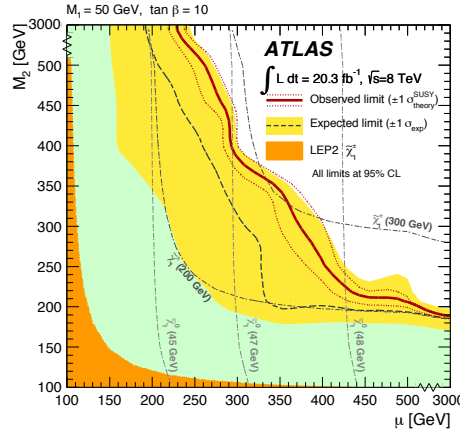
(b) pMSSM $\tilde{\ell}_R$, $M_1=140$ GeV



(c) pMSSM $\tilde{\ell}_R$, $M_1=250$ GeV



(d) pMSSM $\tilde{\tau}_R$, $M_1=75$ GeV



(e) pMSSM no $\tilde{\ell}$, $M_1=50$ GeV

Figure 8. Observed and expected 95% CL exclusion contours in the pMSSM model with (a)–(c) sleptons, (d) staus and (e) no sleptons. The band around the expected limit shows the $\pm 1\sigma$ variations of the expected limit, including all uncertainties except theoretical uncertainties on the signal cross-section. The dotted lines around the observed limit indicate the sensitivity to $\pm 1\sigma$ variations of these theoretical uncertainties. The area covered by the -1σ expected limit is shown in green. The blue contours in (a)–(c) correspond to the 7 TeV limits from the ATLAS three-lepton analysis [17]. Linear interpolation is used to account for the discrete nature of the signal grids.

10 Acknowledgements

We thank CERN for the very successful operation of the LHC, as well as the support staff from our institutions without whom ATLAS could not be operated efficiently.

We acknowledge the support of ANPCyT, Argentina; YerPhI, Armenia; ARC, Australia; BMWF and FWF, Austria; ANAS, Azerbaijan; SSTC, Belarus; CNPq and FAPESP, Brazil; NSERC, NRC and CFI, Canada; CERN; CONICYT, Chile; CAS, MOST and NSFC, China; COLCIENCIAS, Colombia; MSMT CR, MPO CR and VSC CR, Czech Republic; DNRF, DNSRC and Lundbeck Foundation, Denmark; EPLANET, ERC and NSRF, European Union; IN2P3-CNRS, CEA-DSM/IRFU, France; GNSF, Georgia; BMBF, DFG, HGF, MPG and AvH Foundation, Germany; GSRT and NSRF, Greece; ISF, MINERVA, GIF, I-CORE and Benoziyo Center, Israel; INFN, Italy; MEXT and JSPS, Japan; CNRST, Morocco; FOM and NWO, Netherlands; BRF and RCN, Norway; MNiSW and NCN, Poland; GRICES and FCT, Portugal; MNE/IFA, Romania; MES of Russia and ROSATOM, Russian Federation; JINR; MSTB, Serbia; MSSR, Slovakia; ARRS and MIZŠ, Slovenia; DST/NRF, South Africa; MINECO, Spain; SRC and Wallenberg Foundation, Sweden; SER, SNSF and Cantons of Bern and Geneva, Switzerland; NSC, Taiwan; TAEK, Turkey; STFC, the Royal Society and Leverhulme Trust, United Kingdom; DOE and NSF, United States of America.

The crucial computing support from all WLCG partners is acknowledged gratefully, in particular from CERN and the ATLAS Tier-1 facilities at TRIUMF (Canada), NDGF (Denmark, Norway, Sweden), CC-IN2P3 (France), KIT/GridKA (Germany), INFN-CNAF (Italy), NL-T1 (Netherlands), PIC (Spain), ASGC (Taiwan), RAL (UK) and BNL (USA) and in the Tier-2 facilities worldwide.

References

- [1] H. Miyazawa, *Baryon Number Changing Currents*, *Prog. Theor. Phys.* **36** (6) (1966) 1266–1276.
- [2] P. Ramond, *Dual Theory for Free Fermions*, *Phys. Rev. D* **3** (1971) 2415–2418.
- [3] Y. A. Gol’fand and E. P. Likhtman, *Extension of the Algebra of Poincare Group Generators and Violation of p Invariance*, *JETP Lett.* **13** (1971) 323–326.
- [4] A. Neveu and J. H. Schwarz, *Factorizable dual model of pions*, *Nucl. Phys. B* **31** (1971) 86–112.
- [5] A. Neveu and J. H. Schwarz, *Quark Model of Dual Pions*, *Phys. Rev. D* **4** (1971) 1109–1111.
- [6] J. Gervais and B. Sakita, *Field theory interpretation of supergauges in dual models*, *Nucl. Phys. B* **34** (1971) 632–639.
- [7] D. V. Volkov and V. P. Akulov, *Is the Neutrino a Goldstone Particle?*, *Phys. Lett. B* **46** (1973) 109–110.
- [8] J. Wess and B. Zumino, *A Lagrangian Model Invariant Under Supergauge Transformations*, *Phys. Lett. B* **49** (1974) 52–54.
- [9] J. Wess and B. Zumino, *Supergauge Transformations in Four-Dimensions*, *Nucl. Phys. B* **70** (1974) 39–50.

- [10] R. Barbieri and G. Giudice, *Upper Bounds on Supersymmetric Particle Masses*, *Nucl. Phys. B* **306** (1988) 63–76.
- [11] B. de Carlos and J. A. Casas, *One loop analysis of the electroweak breaking in supersymmetric models and the fine tuning problem*, *Phys. Lett. B* **309** (1993) 320–328, [[hep-ph/9303291](#)].
- [12] P. Fayet, *Supersymmetry and Weak, Electromagnetic and Strong Interactions*, *Phys. Lett. B* **64** (1976) 159–162.
- [13] P. Fayet, *Spontaneously Broken Supersymmetric Theories of Weak, Electromagnetic and Strong Interactions*, *Phys. Lett. B* **69** (1977) 489–494.
- [14] G. R. Farrar and P. Fayet, *Phenomenology of the Production, Decay, and Detection of New Hadronic States Associated with Supersymmetry*, *Phys. Lett. B* **76** (1978) 575–579.
- [15] P. Fayet, *Relations Between the Masses of the Superpartners of Leptons and Quarks, the Goldstino Couplings and the Neutral Currents*, *Phys. Lett. B* **84** (1979) 416–420.
- [16] S. Dimopoulos and H. Georgi, *Softly Broken Supersymmetry and $SU(5)$* , *Nucl. Phys. B* **193** (1981) 150–162.
- [17] ATLAS Collaboration, *Search for direct production of charginos and neutralinos in events with three leptons and missing transverse momentum in $\sqrt{s} = 7$ TeV pp collisions with the ATLAS detector*, *Phys. Lett. B* **718** (2013) 841–859, [[arXiv:1208.3144](#)].
- [18] ATLAS Collaboration, *Search for direct slepton and gaugino production in final states with two leptons and missing transverse momentum with the ATLAS detector in pp collisions at $\sqrt{s} = 7$ TeV*, *Phys. Lett. B* **718** (2013) 879–901, [[arXiv:1208.2884](#)].
- [19] ATLAS Collaboration, *Search for supersymmetry in events with three leptons and missing transverse momentum in $\sqrt{s} = 7$ TeV pp collisions with the ATLAS detector*, *Phys. Rev. Lett.* **108** (2012) 261804, [[arXiv:1204.5638](#)].
- [20] CMS Collaboration, *Search for electroweak production of charginos and neutralinos using leptonic final states in pp collisions at $\sqrt{s} = 7$ TeV*, *JHEP* **11** (2012) 147, [[arXiv:1209.6620](#)].
- [21] D0 Collaboration, V. Abazov, et al., *Search for associated production of charginos and neutralinos in the trilepton final state using 2.3 fb^{-1} of data*, *Phys. Lett. B* **680** (2009) 34–43, [[arXiv:0901.0646](#)].
- [22] CDF Collaboration, T. Aaltonen, et al., *Search for Supersymmetry in $p\bar{p}$ Collisions at $\sqrt{s} = 1.96$ -TeV Using the Trilepton Signature of Chargino-Neutralino Production*, *Phys. Rev. Lett.* **101** (2008) 251801, [[arXiv:0808.2446](#)].
- [23] LEPSUSYWG, ALEPH, DELPHI, L3 and OPAL experiments *note LEPSUSYWG/01-03.1*, <http://lepsusy.web.cern.ch/lepsusy/Welcome.html>.
- [24] ALEPH Collaboration, S. Schael, et al., *Absolute mass lower limit for the lightest neutralino of the MSSM from e^+e^- data at \sqrt{s} up to 209 GeV*, *Phys. Lett. B* **583** (2004) 247–263.
- [25] CDF Collaboration, J. Abdallah, et al., *Searches for supersymmetric particles in e^+e^- collisions up to 208 GeV and interpretation of the results within the MSSM*, *Eur. Phys. J. C* **31** (2003) 421–479, [[hep-ex/0311019](#)].
- [26] L3 Collaboration, M. Acciarri, et al., *Search for charginos and neutralinos in e^+e^- collisions at $\sqrt{s} = 189$ GeV*, *Phys. Lett. B* **472** (2000) 420–433, [[hep-ex/9910007](#)].

- [27] OPAL Collaboration, G. Abbiendi, et al., *Search for chargino and neutralino production at $\sqrt{s} = 192\text{ GeV}$ to 209 GeV at LEP*, *Eur. Phys. J. C* **35** (2004) 1–20, [[hep-ex/0401026](#)].
- [28] J. Alwall et al., *Simplified Models for a First Characterization of New Physics at the LHC*, *Phys. Rev. D* **79** (2009) 075020, [[arXiv:0810.3921](#)].
- [29] A. Djouadi et al., *The Minimal supersymmetric standard model: Group summary report*, [hep-ph/9901246](#).
- [30] ATLAS Collaboration, *Observation of a new particle in the search for the Standard Model Higgs boson with the ATLAS detector at the LHC*, *Phys. Lett. B* **716** (2012) 1–29, [[arXiv:1207.7214](#)].
- [31] CMS Collaboration, *Observation of a new boson at a mass of 125 GeV with the CMS experiment at the LHC*, *Phys. Lett. B* **716** (2012) 30–61, [[arXiv:1207.7235](#)].
- [32] ATLAS Collaboration, *The ATLAS Experiment at the CERN Large Hadron Collider*, *JINST* **3** (2008) S08003.
- [33] ATLAS Collaboration, *Performance of the ATLAS Trigger System in 2010*, *Eur. Phys. J. C* **72** (2012) 1849, [[arXiv:1110.1530](#)].
- [34] P. Nason, *A New method for combining NLO QCD with shower Monte Carlo algorithms*, *JHEP* **11** (2004) 040, [[hep-ph/0409146](#)].
- [35] S. Frixione, P. Nason, and C. Oleari, *Matching NLO QCD computations with Parton Shower simulations: the POWHEG method*, *JHEP* **11** (2007) 070, [[arXiv:0709.2092](#)].
- [36] ATLAS Collaboration, *Summary of ATLAS Pythia 8 tunes*, *ATL-PHYS-PUB-2012-003*, <https://cdsweb.cern.ch/record/1474107>, (2012).
- [37] H.-L. Lai et al., *New parton distributions for collider physics*, *Phys. Rev. D* **82** (2010) 074024, [[arXiv:1007.2241](#)].
- [38] T. Sjostrand, S. Mrenna, and P. Z. Skands, *PYTHIA 6.4 Physics and Manual*, *JHEP* **05** (2006) 026, [[hep-ph/0603175](#)].
- [39] J. M. Campbell and R. K. Ellis, *An Update on vector boson pair production at hadron colliders*, *Phys. Rev. D* **60** (1999) 113006, [[hep-ph/9905386](#)].
- [40] J. M. Campbell et al., *Vector boson pair production at the LHC*, *JHEP* **07** (2011) 018, [[arXiv:1105.0020](#)].
- [41] S. Frixione and B. R. Webber, *Matching NLO QCD computations and parton shower simulations*, *JHEP* **06** (2002) 029, [[hep-ph/0204244](#)].
- [42] G. Corcella et al., *HERWIG 6: An Event generator for hadron emission reactions with interfering gluons (including supersymmetric processes)*, *JHEP* **01** (2001) 010, [[hep-ph/0011363](#)].
- [43] N. Kauer and G. Passarino, *Inadequacy of zero-width approximation for a light Higgs boson signal*, *JHEP* **08** (2012) 116, [[arXiv:1206.4803](#)].
- [44] ATLAS Collaboration, *ATLAS tunes of PYTHIA 6 and Pythia 8 for MC11*, *ATL-PHYS-PUB-2011-009*, <https://cdsweb.cern.ch/record/1363300>, (2011).
- [45] T. Gleisberg et al., *Event generation with SHERPA 1.1*, *JHEP* **02** (2009) 007, [[arXiv:0811.4622](#)].

- [46] J. Alwall et al., *MadGraph/MadEvent v4: The New Web Generation*, *JHEP* **09** (2007) 028, [[arXiv:0706.2334](#)].
- [47] F. Campanario et al., *QCD corrections to charged triple vector boson production with leptonic decay*, *Phys. Rev.* **D 78** (2008) 094012, [[arXiv:0809.0790](#)].
- [48] J. Pumplin et al., *New generation of parton distributions with uncertainties from global QCD analysis*, *JHEP* **07** (2002) 012, [[hep-ph/0201195](#)].
- [49] S. Dittmaier et al., *Handbook of LHC Higgs Cross Sections: 2. Differential Distributions*, [[arXiv:1201.3084](#)].
- [50] M. L. Mangano et al., *ALPGEN, a generator for hard multiparton processes in hadronic collisions*, *JHEP* **07** (2003) 001, [[hep-ph/0206293](#)].
- [51] A. Kardos et al., *Top quark pair production in association with a Z-boson at NLO accuracy*, *Phys. Rev.* **D 85** (2012) 054015, [[arXiv:1111.0610](#)].
- [52] J. M. Campbell and R. K. Ellis, *$t\bar{t}W^{+-}$ production and decay at NLO*, *JHEP* **07** (2012) 052, [[arXiv:1204.5678](#)].
- [53] J. Campbell, R. K. Ellis, and R. Rontsch, *Single top production in association with a Z boson at the LHC*, *Phys. Rev.* **D87** (2013) 114006, [[arXiv:1302.3856](#)].
- [54] M. Cacciari et al., *Top-pair production at hadron colliders with next-to-next-to-leading logarithmic soft-gluon resummation*, *Phys. Lett.* **B 710** (2012) 612–622, [[arXiv:1111.5869](#)].
- [55] P. Baernreuther, M. Czakon, and A. Mitov, *Percent Level Precision Physics at the Tevatron: First Genuine NNLO QCD Corrections to $q\bar{q} \rightarrow t\bar{t} + X$* , *Phys. Rev. Lett.* **109** (2012) 132001, [[arXiv:1204.5201](#)].
- [56] M. Czakon and A. Mitov, *NNLO corrections to top-pair production at hadron colliders: the all-fermionic scattering channels*, *JHEP* **12** (2012) 054, [[arXiv:1207.0236](#)].
- [57] M. Czakon and A. Mitov, *NNLO corrections to top pair production at hadron colliders: the quark-gluon reaction*, *JHEP* **01** (2013) 080, [[arXiv:1210.6832](#)].
- [58] M. Czakon, P. Fiedler, and A. Mitov, *The total top quark pair production cross-section at hadron colliders through $O(\alpha_S^4)$* , *Phys. Rev. Lett.* **110** (2013) 252004, [[arXiv:1303.6254](#)].
- [59] M. Czakon and A. Mitov, *Top++: A Program for the Calculation of the Top-Pair Cross-Section at Hadron Colliders*, [[arXiv:1112.5675](#)].
- [60] B. P. Kersevan and E. Richter-Was, *The Monte Carlo event generator AcerMC versions 2.0 to 3.8 with interfaces to PYTHIA 6.4, HERWIG 6.5 and ARIADNE 4.1*, *Comput. Phys. Commun.* **184** (2013), no. 3 919 – 985.
- [61] N. Kidonakis, *Next-to-next-to-leading-order collinear and soft gluon corrections for t-channel single top quark production*, *Phys. Rev.* **D 83** (2011) 091503, [[arXiv:1103.2792](#)].
- [62] S. Frixione et al., *Single-top production in MC@NLO*, *JHEP* **03** (2006) 092, [[hep-ph/0512250](#)].
- [63] S. Frixione et al., *Single-top hadron production in association with a W boson*, *JHEP* **07** (2008) 029, [[arXiv:0805.3067](#)].
- [64] N. Kidonakis, *NNLL resummation for s-channel single top quark production*, *Phys. Rev.* **D 81** (2010) 054028, [[arXiv:1001.5034](#)].

- [65] N. Kidonakis, *Two-loop soft anomalous dimensions for single top quark associated production with a W^- or H^-* , *Phys. Rev. D* **82** (2010) 054018, [[arXiv:1005.4451](#)].
- [66] S. Catani et al., *Vector boson production at hadron colliders: A Fully exclusive QCD calculation at NNLO*, *Phys. Rev. Lett.* **103** (2009) 082001, [[arXiv:0903.2120](#)].
- [67] A. Martin et al., *Parton distributions for the LHC*, *Eur. Phys. J. C* **63** (2009) 189–285, [[arXiv:0901.0002](#)].
- [68] S. Agostinelli et al., *GEANT4: A simulation toolkit*, *Nucl. Instrum. Meth. A* **506** (2003) 250–303.
- [69] ATLAS Collaboration, *The ATLAS Simulation Infrastructure*, *Eur. Phys. J. C* **70** (2010) 823–874, [[arXiv:1005.4568](#)].
- [70] ATLAS Collaboration, *The simulation principle and performance of the atlas fast calorimeter simulation fastcalosim*, *ATL-PHYS-PUB-2010-013*, <http://cdsweb.cern.ch/record/1300517>, (2010).
- [71] M. Bahr et al., *Herwig++ Physics and Manual*, *Eur. Phys. J. C* **58** (2008) 639–707, [[arXiv:0803.0883](#)].
- [72] W. Beenakker et al., *Squark and gluino production at hadron colliders*, *Nucl. Phys. B* **492** (1997) 51–103, [[hep-ph/9610490](#)].
- [73] B. Fuks, M. Klasen, D. R. Lamprea, and M. Rothering, *Gaugino production in proton-proton collisions at a center-of-mass energy of 8 TeV*, *JHEP* **10** (2012) 081, [[arXiv:1207.2159](#)].
- [74] B. Fuks, M. Klasen, D. R. Lamprea, and M. Rothering, *Precision predictions for electroweak superpartner production at hadron colliders with Resummino*, *Eur. Phys. J. C* **73** (2013) 2480, [[arXiv:1304.0790](#)].
- [75] B. Fuks, M. Klasen, D. R. Lamprea, and M. Rothering, *Revisiting slepton pair production at the Large Hadron Collider*, *JHEP* **01** (2014) 168, [[arXiv:1310.2621](#)].
- [76] M. Kramer et al., *Supersymmetry production cross sections in pp collisions at $\sqrt{s} = 7$ TeV*, [[arXiv:1206.2892](#)].
- [77] ATLAS Collaboration, *Electron performance measurements with the ATLAS detector using the 2010 LHC proton-proton collision data*, *Eur. Phys. J. C* **72** (2012) 1909, [[arXiv:1110.3174](#)].
- [78] ATLAS Collaboration, *Measurement of the inclusive W^\pm and Z/γ^* cross sections in the e and μ decay channels in pp collisions at $\sqrt{s} = 7$ TeV with the atlas detector*, *Phys. Rev. D* **85** (2012) 072004, [[arXiv:1109.5141](#)].
- [79] M. Cacciari, G. P. Salam, and G. Soyez, *The anti- k_t jet clustering algorithm*, *JHEP* **04** (2008) 063, [[arXiv:0802.1189](#)].
- [80] ATLAS Collaboration, *Jet energy measurement with the ATLAS detector in proton-proton collisions at $\sqrt{s} = 7$ TeV*, *Eur. Phys. J. C* **73** (2013) 2304, [[arXiv:1112.6426](#)].
- [81] ATLAS Collaboration, *Single hadron response measurement and calorimeter jet energy scale uncertainty with the ATLAS detector at the LHC*, *Eur. Phys. J. C* **73** (2013) 2305, [[arXiv:1203.1302](#)].
- [82] ATLAS Collaboration, *Commissioning of the ATLAS high-performance b-tagging algorithms in the 7 TeV collision data*, *ATLAS-CONF-2011-102*, <http://cdsweb.cern.ch/record/1369219>, (2011).

- [83] ATLAS Collaboration, *Determination of the tau energy scale and the associated systematic uncertainty in proton-proton collisions at $\sqrt{s} = 8$ TeV with the ATLAS detector at the LHC in 2012*, ATLAS-CONF-2013-044 (2013).
- [84] ATLAS Collaboration, *Performance of missing transverse momentum reconstruction in proton-proton collisions at 7 TeV with ATLAS*, *Eur. Phys. J. C* **72** (2012) 1844, [[arXiv:1108.5602](#)].
- [85] ATLAS Collaboration, *Identification of the hadronic decays of tau leptons in 2012 data with the ATLAS detector*, ATLAS-CONF-2013-064 (2013).
- [86] C. Lester and D. Summers, *Measuring masses of semiinvisibly decaying particles pair produced at hadron colliders*, *Phys. Lett. B* **463** (1999) 99–103, [[hep-ph/9906349](#)].
- [87] A. Barr, C. Lester, and P. Stephens, *$m(T\bar{T})$: The Truth behind the glamour*, *J. Phys. G* **29** (2003) 2343–2363, [[hep-ph/0304226](#)].
- [88] ATLAS Collaboration, *Measurement of the top quark-pair production cross section with ATLAS in pp collisions at $\sqrt{s} = 7$ TeV*, *Eur. Phys. J. C* **71** (2011) 1577, [[arXiv:1012.1792](#)].
- [89] ATLAS Collaboration, *Improved luminosity determination in pp collisions at $\sqrt{s} = 7$ TeV using the ATLAS detector at the LHC*, *Eur. Phys. J. C* **73** (2013) 2518, [[arXiv:1302.4393](#)].
- [90] ATLAS Collaboration, *Measurement of WZ production in proton-proton collisions at $\sqrt{s} = 7$ TeV with the ATLAS detector*, *Eur. Phys. J. C* **72** (2012) 2173, [[arXiv:1208.1390](#)].
- [91] ATLAS Collaboration, *Measurement of ZZ production in pp collisions at $\sqrt{s} = 7$ TeV and limits on anomalous ZZZ and $ZZ\gamma$ couplings with the ATLAS detector*, *JHEP* **03** (2013) 128, [[arXiv:1211.6096](#)].
- [92] A. L. Read, *Presentation of search results: The $CL(s)$ technique*, *J. Phys. G* **28** (2002) 2693–2704.
- [93] G. Cowan et al., *Asymptotic formulae for likelihood-based tests of new physics*, *Eur. Phys. J. C* **71** (2011) 1554, [[arXiv:1007.1727](#)].

The ATLAS Collaboration

G. Aad⁸⁴, T. Abajyan²¹, B. Abbott¹¹², J. Abdallah¹⁵², S. Abdel Khalek¹¹⁶, O. Abdinov¹¹, R. Aben¹⁰⁶, B. Abi¹¹³, M. Abolins⁸⁹, O.S. AbouZeid¹⁵⁹, H. Abramowicz¹⁵⁴, H. Abreu¹³⁷, Y. Abulaiti^{147a,147b}, B.S. Acharya^{165a,165b,a}, L. Adamczyk^{38a}, D.L. Adams²⁵, J. Adelman¹⁷⁷, S. Adomeit⁹⁹, T. Adye¹³⁰, T. Agatonovic-Jovin^{13b}, J.A. Aguilar-Saavedra^{125f,125a}, M. Agustoni¹⁷, S.P. Ahlen²², A. Ahmad¹⁴⁹, F. Ahmadov^{64,b}, G. Aielli^{134a,134b}, T.P.A. Åkesson⁸⁰, G. Akimoto¹⁵⁶, A.V. Akimov⁹⁵, J. Albert¹⁷⁰, S. Albrand⁵⁵, M.J. Alconada Verzini⁷⁰, M. Aleksa³⁰, I.N. Aleksandrov⁶⁴, C. Alexa^{26a}, G. Alexander¹⁵⁴, G. Alexandre⁴⁹, T. Alexopoulos¹⁰, M. Alhroob^{165a,165c}, G. Alimonti^{90a}, L. Alio⁸⁴, J. Alison³¹, B.M.M. Allbrooke¹⁸, L.J. Allison⁷¹, P.P. Allport⁷³, S.E. Allwood-Spiers⁵³, J. Almond⁸³, A. Aloisio^{103a,103b}, R. Alon¹⁷³, A. Alonso³⁶, F. Alonso⁷⁰, C. Alpigiani⁷⁵, A. Altheimer³⁵, B. Alvarez Gonzalez⁸⁹, M.G. Alviggi^{103a,103b}, K. Amako⁶⁵, Y. Amaral Coutinho^{24a}, C. Amelung²³, D. Amidei⁸⁸, V.V. Ammosov^{129,*}, S.P. Amor Dos Santos^{125a,125c}, A. Amorim^{125a,125b}, S. Amoroso⁴⁸, N. Amram¹⁵⁴, G. Amundsen²³, C. Anastopoulos¹⁴⁰, L.S. Ancu¹⁷, N. Andari³⁰, T. Andeen³⁵,

Simplified Model	$m_{\tilde{\chi}_1^0}, m_{\tilde{\chi}_2^0}$ [GeV]	$\sigma(pp \rightarrow \tilde{\chi}_1^\pm \tilde{\chi}_2^0)$ [pb]	Generated Events (raw) multiplicity	Signal Region	Expected events for 20.3 fb ⁻¹					
					Lepton requirement	SFOS	b -tagged jet veto	E_T^{miss}	m_T	3ℓ Z veto
$\tilde{\ell}_L$ -mediated	267.5, 232.5	0.24±0.02	39999	SR0 τa -bin1	165	116	111	29	27	27
$\tilde{\ell}_L$ -mediated				SR0 τa -bin2	165	116	111	17	13	13
$\tilde{\ell}_L$ -mediated				SR0 τa -bin3	165	116	111	22	1.1	1.1
$\tilde{\ell}_L$ -mediated				SR0 τa -bin4	165	116	111	24	5	5
$\tilde{\ell}_L$ -mediated	407.5, 342.5	0.036±0.003	40000	SR0 τa -bin5	63	28	27	6	4	3.3
$\tilde{\ell}_L$ -mediated				SR0 τa -bin6	63	28	27	8	4	4
$\tilde{\ell}_L$ -mediated				SR0 τa -bin7	63	28	27	12	4	4
$\tilde{\ell}_L$ -mediated				SR0 τa -bin8	63	28	27	2	1.5	1.5
WZ -mediated	175.0, 100.0	1.35±0.09	20000	SR0 τa -bin9	148	78	75	20	13	10
WZ -mediated				SR0 τa -bin10	148	78	75	20	7	7
WZ -mediated				SR0 τa -bin11	148	78	75	19	15	15
WZ -mediated				SR0 τa -bin12	148	78	75	19	4	4
WZ -mediated	350.0, 50.0	0.074±0.005	20000	SR0 τa -bin13	11	10	10	1.1	0.6	0.6
WZ -mediated				SR0 τa -bin14	11	10	10	8	2.4	2.4
WZ -mediated				SR0 τa -bin15	11	10	10	2.9	1.6	1.6
WZ -mediated				SR0 τa -bin16	11	10	10	7	5	4.8
$\tilde{\ell}_L$ -mediated	687.5, 62.5	0.0020±0.0002	39899	SR0 τa -bin17	5	5	4	1.4	0.5	0.5
$\tilde{\ell}_L$ -mediated				SR0 τa -bin18	5	5	4	1.4	0.9	0.9
$\tilde{\ell}_L$ -mediated				SR0 τa -bin19	5	5	4	3.0	0.23	0.23
$\tilde{\ell}_L$ -mediated				SR0 τa -bin20	5	5	4	3.0	2.7	2.7

Expected number of events from representative SUSY signal models with high sensitivity in SR0 τa . The decay modes of the charginos and neutralinos is indicated as well as their masses and production cross-sections. The number of events expected for a luminosity of 20.3 fb⁻¹ is quoted at each step of the selection.

Model	Simplified Wh -mediated	Simplified Wh -mediated	Simplified $\tilde{\tau}_L$ -mediated	Simplified Wh -mediated
$m_{\tilde{\chi}_1^0}, m_{\tilde{\chi}_2^0}$ [GeV]	0, 130	10, 140	275, 25	0, 130
$\sigma(pp \rightarrow \tilde{\chi}_1^\pm \tilde{\chi}_2^0)$ [pb]	4.24±0.29	3.20±0.22	0.216±0.015	4.24±0.29
Generated Events (raw)	20000	20000	20000	20000
Expected events for 20.3 fb ⁻¹				
Signal Region	SR0 τb	SR1 τ	SR2 τa	SR2 τb
Lepton multiplicity	19	23	48	34
Z veto	--	22	--	--
b -tagged jet veto	18	21	46	33
E_T^{miss}	12	14	35	14
m_{T2}^{max}	--	--	14	--
$\sum p_T^\ell$	--	10	--	--
$p_{T,2}^{\text{nd } \ell}$	--	6	--	--
$m_{\ell\tau}$	--	6	--	--
$m_{\tau\tau}$	--	--	--	10
$\sum p_T^\tau$	--	--	--	5
$p_T^{3\text{rd } \ell}$	7	--	--	--
$\min(\Delta\phi(\ell^\pm, \ell^\mp))$	5	--	--	--

Expected number of events from representative SUSY signal models with high sensitivity in SR0 τb , SR1 τ , SR2 τa and SR2 τb . The decay mode, as well as the masses and production cross-sections are indicated. The number of events expected for a luminosity of 20.3 fb⁻¹ is quoted at each step of the selection.